Published for SISSA by Springer

Received: *August 15, 2025*
Accepted: *November 6, 2025*
Published: *December 23, 2025*

Search for a new scalar resonance decaying to a Higgs boson and another new scalar particle in the final state with two bottom quarks and two photons in proton-proton collisions at $\sqrt{s} = 13$ TeV

The CMS collaboration

E-mail: cms-publication-committee-chair@cern.ch

Abstract: A search is presented for a new scalar resonance, X, decaying to a standard model Higgs boson and another new scalar particle, Y, in the final state where the Higgs boson decays to a $b\bar{b}$ pair, while the Y particle decays to a pair of photons. The search is performed in the mass range 240–1000 GeV for the resonance X, and in the mass range 70–800 GeV for the particle Y, using proton-proton collision data collected by the CMS experiment at $\sqrt{s} = 13$ TeV, corresponding to an integrated luminosity of 132 fb^{-1}. In general, the data are found to be compatible with the standard model expectation. Observed (expected) upper limits at 95% confidence level on the product of the production cross section and the relevant branching fraction are extracted for the $X \to YH$ process, and are found to be within the range of 0.05–2.69 (0.08–1.94) fb, depending on m_X and m_Y. The most significant deviation from the background-only hypothesis is observed for X and Y masses of 300 and 77 GeV, respectively, with a local (global) significance of 3.33 (0.65) standard deviations.

Keywords: Beyond Standard Model, Hadron-Hadron Scattering, Higgs Physics, Particle and Resonance Production

ArXiv ePrint: 2508.11494

https://doi.org/10.1007/JHEP12(2025)178

Contents

1 Introduction **1**

2 The CMS detector and event reconstruction **3**

3 Data and simulated samples **5**

4 Analysis strategy and event categorization **6**
4.1 Event preselection 6
4.2 Estimation of backgrounds with misidentified photons from data 8
4.3 Parametric neural network selection 9
4.4 Event categorization 11

5 Signal and background modeling **12**
5.1 Signal modeling 12
5.2 Background modeling 12

6 Systematic uncertainties **14**
6.1 Theoretical uncertainties 15
6.2 Experimental uncertainties 16

7 Results **17**

8 Summary **20**

The CMS collaboration **27**

JHEP12(2025)178

1 Introduction

Since the discovery of a Higgs boson by the ATLAS and CMS Collaborations at the CERN LHC in 2012 [1–3], an extensive campaign of experimental investigations has been launched to determine its properties. The latest results from these studies have been published by the two collaborations in 2022 [4, 5]. The Higgs boson properties that have been measured with the current data sets are compatible with the standard model (SM) prediction.

Despite the progress in studying the characteristics of the Higgs boson, there are still some open questions related to its nature, e.g., the hierarchy problem — the question of why the Higgs mass is so much smaller than the Planck scale. Also, the SM is not a complete theory as it has no explanations for neutrino masses and the origin of dark matter. Such shortcomings could be addressed by theoretical models beyond the SM (BSM).

One of these BSM theories is supersymmetry (SUSY) [6–13], which predicts the existence of partners for each SM particle having the same properties as their SM counterparts but differing in mass and spin. By extending the SM in this way, SUSY offers a solution to the hierarchy problem, provides an explanation for the nature of dark matter, and modifies

the running of the coupling constants of the fundamental forces so that they approximately converge to a common value at a very large energy scale, as predicted by grand unified theories.

In its simplest form, denoted as the minimal supersymmetric SM (MSSM) [14], SUSY requires the introduction of one additional Higgs SU(2)-doublet, leading to the prediction of five Higgs boson mass eigenstates, instead of only one as in the SM. The MSSM Lagrangian contains a supersymmetric mass term for these Higgs doublets associated with a mass parameter, μ_{SUSY}, that has to be at the scale of the SUSY breaking, m_{SUSY}, to explain the observed phenomenology. However, there is no strong theoretical reason in the MSSM for μ_{SUSY} and m_{SUSY} to be of the same order. This "necessary accident" of the MSSM is called the "μ-problem", and can be resolved in further extensions of the model. More specifically, the next-to-MSSM (NMSSM) [15] introduces an additional Higgs singlet field, S, which provides an explanation for the origin and the scale of the μ_{SUSY} term.

Because of the existence of the extra singlet field, the NMSSM Higgs sector ends up having seven gauge eigenstates. The gauge eigenstates combine to form seven mass eigenstates: three CP-even (H_1, H_2, H_3), two CP-odd (A_1, A_2), and two charged ($\mathrm{H}^{\pm}$), where the subscripts indicate the mass ordering. In the so-called alignment limit, the heavier neutral eigenstates only weakly couple to the 125 GeV Higgs boson (H) observed at the LHC, and, thus, their decay to HH is suppressed. In this scenario, decays of the form $\mathrm{X} \to \mathrm{YH}$, where X is one of the heaviest neutral eigenstates (H_3 or A_2) and Y is a lighter one, are preferred, and motivate the search presented in this paper. A complete picture of the NMSSM theory is given in ref. [15].

Another category of BSM models with the potential to explain some of the SM shortcomings is the two-real-scalar-singlet model (TRSM). More concretely, in the specific extension of TRSM detailed in ref. [16], the asymmetric signature with one SM Higgs boson and one new scalar resonance (Y) can occur. The main difference with the NMSSM is that, in the TRSM, the additional scalars (X and Y) have SM Higgs boson branching fractions ($\mathcal{B}$), which implies a small $\mathcal{B}(\mathrm{Y} \to \gamma\gamma)$, while in the NMSSM there is more freedom for this branching fraction to take a wide range of possible values. Further details and benchmarks for the models discussed above are given in ref. [17].

We note that this search probes the $\mathrm{X} \to \mathrm{YH}$ final state in a model-independent way. The X and Y particles are taken to be scalar, and we further assume that the narrow-width approximation is applicable. The connection to the aforementioned models can be recovered by appropriately matching the X and Y particles to scalars in the mass hierarchy of each model.

Different combinations of $\mathrm{X} \to \mathrm{YH}$ final states have been studied by the CMS Collaboration: $\mathrm{Y} \to \mathrm{b\bar{b}}$ and $\mathrm{H} \to \mathrm{b\bar{b}}$ [18]; $\mathrm{Y} \to \mathrm{b\bar{b}}$ and $\mathrm{H} \to \tau\tau$ [19]; $\mathrm{Y} \to \tau\tau$ and $\mathrm{H} \to \gamma\gamma$, and $\mathrm{Y} \to \gamma\gamma$ and $\mathrm{H} \to \tau\tau$ [20]; as well as $\mathrm{Y} \to \mathrm{b\bar{b}}$ and $\mathrm{H} \to \gamma\gamma$ [21]. The search described in this paper probes the so far unexplored $\mathrm{Y} \to \gamma\gamma$ and $\mathrm{H} \to \mathrm{b\bar{b}}$ final state (figure 1) for masses of the X scalar between 240 and 1000 GeV and masses of the Y scalar satisfying the condition $m_{\mathrm{X}} > m_{\mathrm{Y}} + m_{\mathrm{H}}$, with $m_{\mathrm{Y}} > 70$ GeV. The mass range is chosen based on several considerations, including detector sensitivity at low masses and the need for a different set of reconstruction techniques at higher mass, adjusted for boosted topologies. Additionally, the condition $m_{\mathrm{X}} > m_{\mathrm{Y}} + m_{\mathrm{H}}$ ensures that the decay $\mathrm{X} \to \mathrm{Y}H$ is kinematically allowed. This final state is well motivated by the high $\mathcal{B}(\mathrm{H} \to \mathrm{b\bar{b}})$ and the clean signature of the photon pair.

JHEP12(2025)178

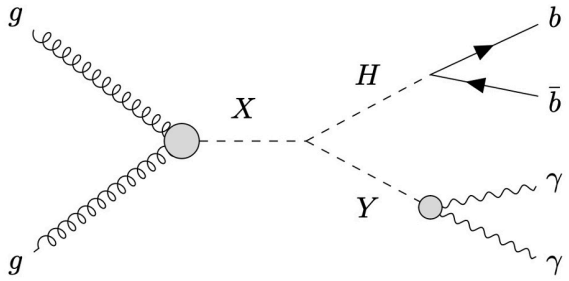

Figure 1. Feynman diagram for the production of the BSM resonance X and its subsequent decay to two scalars, one SM Higgs boson and one BSM scalar Y, with $H \to b\bar{b}$ and $Y \to \gamma\gamma$.

Apart from theoretical considerations, this search is also prompted by excesses observed in similar analyses searching for new resonances in signatures with Higgs bosons. The search for $X \to Y(b\bar{b})H(\gamma\gamma)$ (same final state as this analysis but with inverted decays modes for Y and H) has observed a local (global) excess of 3.8 (2.8) standard deviations for $m_X = 650\,\text{GeV}$ and $m_Y = 90\,\text{GeV}$ [21]. Under the assumption that the Y can also decay to a pair of photons and that the branching fractions of $Y \to \gamma\gamma$ and $Y \to b\bar{b}$ are the same as those of the Higgs boson, as predicted in the TRSM, this excess can be probed by this search. Moreover, a search for an additional, SM-like, low-mass Higgs boson in the $H \to \gamma\gamma$ channel found an excess of local (global) significance of 2.9 (1.3) standard deviations at 95.4 GeV [22].

The paper is structured as follows: section 2 gives a description of the CMS detector and the event reconstruction. The data sets and simulated samples used in the analysis are detailed in section 3. Section 4 describes general analysis strategy, the event selection and categorization, and section 5 outlines the modeling of the signal and the background. The systematic uncertainties are discussed in section 6. Finally, results are presented in section 7, and the analysis is summarized in section 8. The results of the analysis are provided in tabulated form in the HEPData record [23].

2 The CMS detector and event reconstruction

The central feature of the CMS apparatus is a superconducting solenoid of 6 m internal diameter, providing a magnetic field of 3.8 T. Within the solenoid volume are a silicon pixel and strip tracker, a lead tungstate crystal electromagnetic calorimeter (ECAL), and a brass and scintillator hadron calorimeter (HCAL), each composed of a barrel and two endcap sections. Forward calorimeters extend the pseudorapidity coverage provided by the barrel and endcap detectors. Muons are reconstructed in gas-ionization detectors embedded in the steel flux-return yoke outside the solenoid. More detailed descriptions of the CMS detector, together with a definition of the coordinate system used and the relevant kinematic variables, can be found in refs. [24, 25].

Events of interest are selected using a two-tiered trigger system. The first level (L1), composed of custom hardware processors, uses information from the calorimeters and muon detectors to select events at a rate of around 100 kHz within a fixed latency of about 4 μs [26]. The second level, known as the high-level trigger (HLT), consists of a farm of processors

JHEP12(2025)178

running a version of the full event reconstruction software optimized for fast processing, and reduces the event rate to around 1 kHz before data storage [27, 28].

The primary vertex (PV) is taken to be the vertex corresponding to the hardest scattering in the event, evaluated using tracking information alone, as described in section 9.4.1 of ref. [29]. As a consequence of the presence of jets from the $H \to b\bar{b}$ decay, this approach provides a similar or better $m_{\gamma\gamma}$ resolution to that obtained in $H \to \gamma\gamma$ analyses using a customized vertex finding method. A particle-flow (PF) algorithm [30] aims to reconstruct and identify each individual particle in the event, with an optimized combination of information from the various elements of the CMS detector in the following paragraphs.

The energy of photons is obtained from the ECAL measurement. In the barrel section of the ECAL, an energy resolution of about 1% is achieved for unconverted or late-converting photons in the tens of GeV energy range. The energy resolution of the remaining barrel photons is about 1.3% up to absolute pseudorapidity $|\eta| = 1$, changing to about 2.5% at $|\eta| = 1.4$. In the endcaps, the energy resolution is about 2.5% for unconverted or late-converting photons, and between 3 and 4% for the other ones [31]. The diphoton mass resolution, as measured in $H \to \gamma\gamma$ decays, is typically in the 1–2% range, depending on the measurement of the photon energies in the ECAL and the topology of the photons in the event [32].

The energy of electrons is determined from a combination of the electron momentum at the PV, as determined by the tracker, the energy of the corresponding ECAL cluster, and the energy sum of all bremsstrahlung photons spatially compatible with originating from the electron track. The momentum resolution for electrons with transverse momentum $p_T \approx 45\,\text{GeV}$ from $Z \to e^+e^-$ decays ranges from 2 to 5%. It is generally better in the barrel region than in the endcaps, and also depends on the bremsstrahlung energy emitted by the electron as it traverses the material in front of the ECAL [33, 34].

The energy of muons is obtained from the curvature of the corresponding track. Muons are measured in the pseudorapidity range $|\eta| < 2.4$, with detection planes made using three technologies: drift tubes, cathode strip chambers, and resistive-plate chambers. Matching muons to tracks measured in the silicon tracker results in a relative transverse momentum resolution, for muons with $20 < p_T < 100\,\text{GeV}$, of 1.3–2.0% in the barrel and better than 6% in the endcaps. Measurements made with cosmic ray muons show that, in the central region of the detector, the p_T resolution is better than 10% for muons with p_T up to 1 TeV [35].

The energy of charged hadrons is determined from a combination of their momentum measured in the tracker and the matching ECAL and HCAL energy deposits, corrected for the response function of the calorimeters to hadronic showers. The energy of neutral hadrons is obtained from the corresponding corrected ECAL and HCAL energies.

Jets are reconstructed offline using the anti-k_T algorithm [36, 37] with a distance parameter of 0.4. Jet momentum is determined as the vectorial sum of all PF object momenta in the jet, and is found from simulation to be, on average, within 5 to 10% of the true momentum over the entire p_T spectrum and detector acceptance. Pileup, referring to additional proton-proton (pp) interactions within the same or nearby bunch crossings (pileup), can contribute additional tracks and calorimetric energy depositions, thereby increasing the apparent jet momentum. To mitigate this effect, tracks identified to be originating from pileup vertices are discarded and an offset correction is applied to correct for remaining contributions [38]. Jet energy

JHEP12(2025)178

corrections are derived from simulation studies so that the average measured energy of jets becomes identical to that of particle-level jets. In situ measurements of the momentum balance in dijet, photon + jet, Z + jet, and multijet events are used to determine any residual differences between the jet energy scale in data and in simulation, and appropriate corrections are made [39]. Additional selection criteria are applied to each jet to remove jets potentially dominated by instrumental effects or reconstruction failures [38]. The identification of b quark jets uses the DeepJet algorithm [40, 41]. In this analysis, no explicit requirement is placed on the DeepJet score; instead the continuous distribution of the DeepJet score is used as an input to the multivariate discriminator used for the final event selection, as discussed in sections 4.1 and 4.3.

The PF isolation of an object is quantified by the p_{T} sum of other PF objects within a cone $\Delta R = \sqrt{(\Delta\eta)^2 + (\Delta\phi)^2}$ around its direction, where ϕ is the azimuthal angle. The cut-off value chosen for ΔR depends on the type of object.

3 Data and simulated samples

This search uses pp collision data recorded in 2016–2018 by the CMS experiment at the LHC. The data are collected by L1 and HLT algorithms that require at least two photons satisfying $p_{\mathrm{T}} > 30\,\mathrm{GeV}$ for the leading- and $p_{\mathrm{T}} > 18\,\mathrm{GeV}$ for the subleading-p_{T} photon, respectively, and a diphoton invariant mass $m_{\gamma\gamma} > 55\,\mathrm{GeV}$. Additional criteria are applied by the trigger algorithms on the photons based on the shower profiles in the calorimeter, the ratio of the energy deposition in the HCAL to that in the ECAL, and the isolation of the photons from PF objects in the same event. Details will be further discussed in section 4.1. The integrated luminosity associated with the data set is $132\,\mathrm{fb}^{-1}$.

In all simulated samples discussed below, parton showering, fragmentation with the standard p_{T}-ordered parton shower scheme, as well as the underlying event description, are modeled using pythia 8.240 with the CP5 tune [42, 43]. The NNPDF 3.1 set [44] is used to describe the parton distribution functions, and the Geant4 package [45] is used to model the detector response.

Only the gluon-gluon fusion process is considered for the production of X in the simulated signal samples. These samples are generated with MadGraph5_aMC@NLO v2.6.5 at leading order (LO) precision [46, 47]. The new scalar bosons in the signal are simulated as CP-even, and the product of the signal production cross section and its branching fraction to the $\mathrm{Y} \to \gamma\gamma$ and $\mathrm{H} \to \mathrm{b\bar{b}}$ final state is normalized to 1 fb. As already mentioned, we assume that the narrow-width approximation holds, i.e., the particle decay width is small compared to its mass. As a consequence, possible interference with any type of background process is ignored.

The SM production of single Higgs bosons decaying to a pair of photons constitutes a resonant background for this search. To model this background we utilize simulated samples for the production of Higgs bosons via gluon-gluon and vector boson fusion, as well as associated production of Higgs bosons with vector bosons or with a top quark-antiquark pair ($\mathrm{t\bar{t}H}$). In all of these samples the Higgs boson is forced to decay into two photons. These Monte Carlo samples are generated with MadGraph5_aMC@NLO v2.6.5 at NLO in quantum chromodynamics (QCD), with cross sections and decay branching fraction taken from ref. [48]. Contributions from other single H production modes are negligible and,

JHEP12(2025)178

therefore, omitted. Although less important, we also consider the contribution of gluon-gluon fusion Higgs pair production. It is generated with the POWHEG 2 [49–52] program at next-to-leading order (NLO) precision in perturbative QCD [53–57], including the full top quark mass dependence [58].

The rest of the resonant (Drell-Yan and dibosons) and all the nonresonant background processes are estimated from data. However, simulated samples are used for the optimization of the analysis strategy. The Drell-Yan (DY) simulated sample is generated using POWHEG 2 at NLO in perturbative QCD, and the diboson VV, where $\mathrm{V} = \mathrm{W}, \mathrm{Z}$, samples are generated using either MADGRAPH5_aMC@NLO v2.6.5 or POWHEG 2 at NLO in QCD. The irreducible nonresonant prompt diphoton process ($\gamma\gamma$ + jets) is modeled with SHERPA v.2.2.1 [59] at LO including the box processes, with up to three additional jets in the final state. The reducible nonresonant background from γ + jets events is modeled with PYTHIA 8 [60] at LO. Less important nonresonant backgrounds include $\mathrm{V}+\gamma$, $\mathrm{t\bar{t}}+\gamma$, $\mathrm{t\bar{t}}+\gamma\gamma$, $\mathrm{t\bar{t}V}$, and tZq and are simulated at NLO in QCD using MADGRAPH5_aMC@NLO v2.6.5, except for $\mathrm{t\bar{t}}$, which uses MADGRAPH5_aMC@NLO v2.6.1.

Pileup interactions are taken into account by adding simulated minimum bias interactions to all the generated event samples. The pileup distribution is weighted to match that observed in the data. The mean value of pileup multiplicity ranges from 23 to 32, depending on the year of data taking.

4 Analysis strategy and event categorization

The analysis probes a wide range of signal hypotheses (mass points), and its strategy is built around the necessity to be sensitive for all of them. The baseline selection, denoted as "preselection" below, applies to all of the mass points. It relies on a series of selection criteria on individual photons and photon pairs, and on loose requirements on individual jets and dijet pairs. The preselected events are then given as input to a parametric neural network (PNN), described in detail in section 4.3. The PNN is able to produce a separate output score optimized for each mass point it has been trained on, as well as for intermediate mass points. This dedicated output score is then used to split events in different signal regions (SRs), in order to create categories with high sensitivity for each mass point. In these SRs, the signal manifests as a mass peak in the $m_{\gamma\gamma}$ spectrum, at different values depending on the value of m_{Y} for each mass point. The signal and background models are fitted together and compared to the data. In the absence of significant deviations from the SM prediction, we set an upper limit on the product of the cross section and branching fraction at a wide range of mass points, exploiting the interpolating capabilities of the PNN.

4.1 Event preselection

The analysis preselection largely follows the trigger selection. The first step consists of selecting events with at least two photon candidates each with $p_{\mathrm{T}} > 18\,\mathrm{GeV}$ and with calorimeter superclusters within the ECAL barrel or endcap acceptance. To reduce backgrounds, we impose additional requirements on these photon candidates. The ratio of the energy deposited in the HCAL to that in the ECAL must satisfy $H/E < 0.08$, effectively suppressing the contribution from QCD processes. To reduce backgrounds from DY and VV processes, with

JHEP12(2025)178

$\lvert\eta\rvert$	R_9	$\sigma_{i\eta i\eta}$	I_{ph} [GeV]	I_{tk} [GeV]
Barrel	[0.50,0.85]	<0.015	$<4.0+0.17\rho$	<6.0
	>0.85	—	—	—
Endcap	[0.80,0.90]	<0.035	$<4.0+0.13\rho$	<6.0
	>0.90	—	—	—

Table 1. Additional photon requirements, as functions of $|\eta|$ and R_9. The variable ρ is the median of the transverse energy density per unit area in the event.

electrons mimicking the photon signature, we apply a requirement that there cannot be a charged track reconstructed in the silicon pixel tracker that points to the photon cluster. A photon candidate for which the associated supercluster is close to a track that is compatible with an electron is also rejected. This further reduces the contamination from misidentified electron backgrounds.

Isolation requirements on photons are applied separately to the charged hadron (I_{ch}), photon (I_{ph}), and the track (I_{tk}) components of the photon PF isolation, calculated within a cone of $\Delta R = 0.3$ centered around the photon. Two other variables, R_9 and $\sigma_{i\eta i\eta}$, are commonly used when photons are present in the final state. The variable R_9 is defined as the energy sum of the 3×3 crystals centered around the most energetic crystal, divided by the energy of the photon. The variable $\sigma_{i\eta i\eta}$ is the energy-weighted spread in the η direction of the 5×5 crystals centered around the most energetic crystal. A series of requirements are applied on the above variables to identify the photon candidates in this analysis, matching the online selection. Every photon is required to fulfill $I_{\text{ch}} < 20\,\text{GeV}$, or $I_{\text{ch}}/p_{\text{T}} < 0.3$, or $R_9 > 0.8$. Additional requirements are applied with different values based on the photon candidate $|\eta|$ and R_9 variables, as summarized in table 1. These requirements provide approximately 60% rejection for backgrounds with misidentified photons, with approximately 2% loss of signal efficiency.

Finally, a multivariate algorithm ("photon MVA ID") is used to further select photon candidates. The photon MVA ID is a general-purpose identification variable designed to distinguish photons from jets. It is computed based on multiple photon characteristics that describe the properties of the photon electromagnetic shower and isolation [33]. We impose a photon MVA ID requirement (working point, WP) that has a 90% efficiency for isolated photons relevant for this analysis.

All of the photon candidates in a given event are paired up in all possible combinations. In each diphoton pair, the photon with the highest (lowest) p_{T} is referred to as the "leading" ("subleading") photon. The leading photon is required to have $p_{\text{T}} > 30\,\text{GeV}$, and the invariant mass of the pair must be larger than 55 GeV. After these selections, the diphoton pair with the highest sum p_{T} is selected as the diphoton pair to be used in the analysis. In the signal, the selected diphoton pair is treated as the Y resonance candidate.

The final state for the signal of interest does not include isolated leptons. To suppress backgrounds with leptons in the final state, we reject events with at least one electron of

$p_T > 10\,\text{GeV}$ or muon of $p_T > 15\,\text{GeV}$ satisfying the criteria described below. Electrons and muons must be within detector acceptance, fulfill tight impact parameter criteria, and be separated from any photon candidate by a distance of $\Delta R > 0.2$. Electrons must also satisfy a requirement on an MVA ID variable, which includes isolation information [33]. The WP of the electron MVA ID is chosen to correspond to the 90% efficiency point. Tight identification criteria are also imposed on muons [61]. Additionally, muon candidates must be reconstructed as "global muons" [61], meaning that tracks associated with them must be found both in the tracker and the muon detectors. Finally, the PF relative isolation for muons is required to be < 0.3, which corresponds to $\sim 98\%$ efficiency.

Events are required to have at least two jets with $|\eta| < 2.4$ and $p_T > 25\,\text{GeV}$, each separated from any photon candidate by a distance $\Delta R > 0.4$. No selection on the DeepJet b tagging score is applied at the preselection stage, to allow the PNN to make a b-jet selection that relies on additional event variables and that can be optimized for each signal mass hypothesis. Instead, jets are sorted according to this score, and the two leading ones based on this sorting are preselected. A tighter jet selection, including additional kinematic requirements, for example on the dijet mass, is performed by the PNN classifier, as discussed in section 4.3. A correction is applied to the entirety of the b tagging discriminant distribution in the simulation to match the one in data. To reject events with severe jet-related mismeasurements due to the presence of cosmic ray muons, beam-gas interactions, or beam halo or calorimetric noise, events in both data and simulation are required to pass dedicated noise-rejecting filters [62].

4.2 Estimation of backgrounds with misidentified photons from data

Typically, simulated samples have difficulties reproducing the behavior and the distributions of events with misidentified photons in data. Moreover, given the large phase space covered by this analysis, the statistical power of samples simulating QCD and γ + jets processes is not always sufficient to provide a representative background sample for the training of the MVA methods at the core of the signal versus background classification used in this analysis.

For these reasons, we implemented an estimation of processes with one or two misidentified photons from control samples in data [63]. This can be accomplished using data events in a misidentified-photon-enriched region, independent of the preselection described in section 4.1, as a proxy for the QCD and γ + jets events passing the preselection. The proxy data set is constructed by selecting events that pass all the preselection requirements, but fail the minimum photon MVA ID score criterion. The event properties used as input to the final MVA-based selection are found to be uncorrelated with the minimum photon MVA ID variable. This proxy data set can then be used, with the small modification described below, in the training of the MVA discriminator described in section 4.3 (the list of training variables is summarized in table 2).

In the proxy data set we replace the photon MVA ID score for the photon failing the photon MVA ID requirement with a new value. This new value is randomly chosen in the range from the lower photon MVA ID score threshold to the photon MVA ID score of the other photon in the event, according to the probability distribution function (PDF) that describes the photon MVA ID scores of misidentified photons, as determined from MC γ + jets

JHEP12(2025)178

events. Finally, to properly inject the data-driven description of the misidentified photons into the preselection, the sample normalization has to be adjusted. This is done by applying an individual weight to each of the events in the proxy dataset to match the photon MVA ID distribution for events in the preselection.

This technique improves the overall agreement between simulated samples and data preselection yields, as well as the description of the individual kinematic distributions, resulting in a better background description for training of the MVA described in the following section. The final estimation and modeling of the backgrounds from processes with misidentified photons is performed directly on the data from sideband regions, as discussed in section 5.2, and hence it is independent of the method described in this section.

4.3 Parametric neural network selection

The signal for this search involves two new resonances with unknown masses that are probed in the mass range of 240–1000 GeV. This creates the necessity to derive optimal discriminators for the vastly different mass points being considered. Given that it is not realistic to train a single NN for each mass point because of the large number of such points, a mass-point-aware NN that can generalize the selection optimally to all of the mass points is preferred. This can be achieved with a PNN [64], as described below.

An NN is a function, $f(\vec{x})$, that outputs a score reflecting the similarity of an event, described by the set of input features $\vec{x}$, to signal-like characteristics. A set of such functions $\{f^1, f^2, \ldots\}$, where f^i is an NN trained on $(m_{\mathrm{X}}^i, m_{\mathrm{Y}}^i)$, may be assembled to create $f(\vec{x}; m_{\mathrm{X}}, m_{\mathrm{Y}})$:

$$f\left(\vec{x}; m_{\mathrm{X}}, m_{\mathrm{Y}}\right) = \begin{cases} f^1(\vec{x}) & \text{if } (m_{\mathrm{X}}^1, m_{\mathrm{Y}}^1), \\ f^2(\vec{x}) & \text{if } (m_{\mathrm{X}}^2, m_{\mathrm{Y}}^2), \\ \ldots \end{cases} \tag{4.1}$$

When training a PNN, the target function is $f(\vec{x}; m_{\mathrm{X}}, m_{\mathrm{Y}})$, i.e., a single function, which, given a value for the m_{X}-m_{Y} pair, will provide an optimal discriminator for the chosen mass points. When using this function, picking a value of m_{X} and m_{Y} is equivalent to picking a particular NN to use. This is achieved in practice by including m_{X} and m_{Y} as additional input features. The training of the PNN uses 50% of the available events in each sample and is performed simultaneously on the 224 simulated signal samples corresponding to different m_{X} and m_{Y} hypotheses. All simulated background samples mentioned in section 3 as well as the backgrounds with misidentified photons, estimated as described in section 4.2, are included in the training. Each signal sample consists of $\mathcal{O}(10^5)$ events, and the number of total background events used in the training is $\mathcal{O}(10^7)$. Different m_{X} and m_{Y} values are randomly assigned to the background events to match the signal points included in training. This procedure ensures that m_{X} and m_{Y} features have no discriminating power between signal and background. Instead, the performance of the PNN per mass point is optimized through the correlation between mass values and the training variables.

In order not to bias the training towards a specific signal mass hypothesis, the signal samples are normalized such that the sum of weights is the same for all mass points. All of the signal mass hypotheses are collectively normalized so that their sum of weights is

JHEP12(2025)178

Category	Variables
Photon-related	$p_{\mathrm{T}}(\gamma\gamma)/m_{\gamma\gamma}$, $p_{\mathrm{T}}(\gamma_1)/m_{\gamma\gamma}$, $p_{\mathrm{T}}(\gamma_2)/m_{\gamma\gamma}$, $\Delta R(\gamma\gamma)$, $\Delta\eta(\gamma\gamma)$
Jet-related	$p_{\mathrm{T}}(j_1)$, $p_{\mathrm{T}}(jj)$, $m(jj)$, $\Delta R(jj)$, $m(j_1)$, b tagging score(j_1), b tagging score(j_2), $\Delta R(\gamma_1, j_1)$, $\Delta R(\gamma_1, j_2)$, $\Delta R(\gamma_2, j_1)$, $\Delta R(\gamma_2, j_2)$
Photon-jet combinations	$\Delta R(\gamma_1, jj)$, $\Delta R(\gamma_2, jj)$, $\Delta R(\gamma\gamma, j_1)$, $\Delta R(\gamma\gamma, j_2)$, $\Delta R(\gamma\gamma, jj)$, $\Delta\eta(\gamma\gamma, jj)$, $\Delta\eta(\gamma\gamma, j_1)$, $\Delta\eta(\gamma_1, j_2)$, $\Delta\phi(\gamma\gamma, jj)$, $\Delta\phi(\gamma\gamma, j_1)$, $\Delta\phi(\gamma\gamma, j_2)$

Table 2. The training variables included as input to the PNN used for the final selection of this search. The symbols γ_1, γ_2 denote the leading and subleading photons, while j_1 and j_2 denote the leading and subleading jets.

the same as the one for the background samples, to enhance the discrimination based on shape differences between signal and background.

The PNN used in this analysis is a feedforward network with 3 layers of 50 nodes. The intermediate layers are activated by exponential linear unit (ELU) functions with a dropout probability of 0.05, while the last layer is activated by a sigmoid function. The learning rate is set to 0.01.

The set of training variables given as input to the PNN consists of the most discriminating variables, identified from studies of separate boosted decision trees (BDTs) trained with a much larger set of variables on a representative subset of signal mass points. The correlation of some of the kinematic variables, such as photon p_{T}, with the diphoton mass is minimized by dividing them by $m_{\gamma\gamma}$. Any variable that is still correlated with the diphoton mass is removed from the set of training variables. This prevents the introduction of peaky features to the otherwise smoothly falling $m_{\gamma\gamma}$ distribution of the nonresonant backgrounds. These features would invalidate the background modeling procedure described in section 5.2. The final list of training variables is shown in table 2.

Before defining the SRs of the search, the PNN output score is transformed for each mass point such that the score distribution of the background from the test data set is constant, i.e., "flat". The new score that results from this procedure is referred to as the "transformed score" and is used for the event categorization below. Placing a threshold on the transformed score is equivalent to placing a threshold on the background efficiency.

We note that simpler classification methods, such as BDTs, were used for a small set of representative mass points to understand the performance gains from using a PNN. BDTs based on a few of the most discriminating variables, effectively emulating a cutoff-based analysis, showed a much worse performance for the majority of the mass points. The BDTs using as input the full list of variables mentioned in table 2 improved the performance for all mass points, making it comparable to the one provided by the PNN up to around 5%, but

JHEP12(2025)178

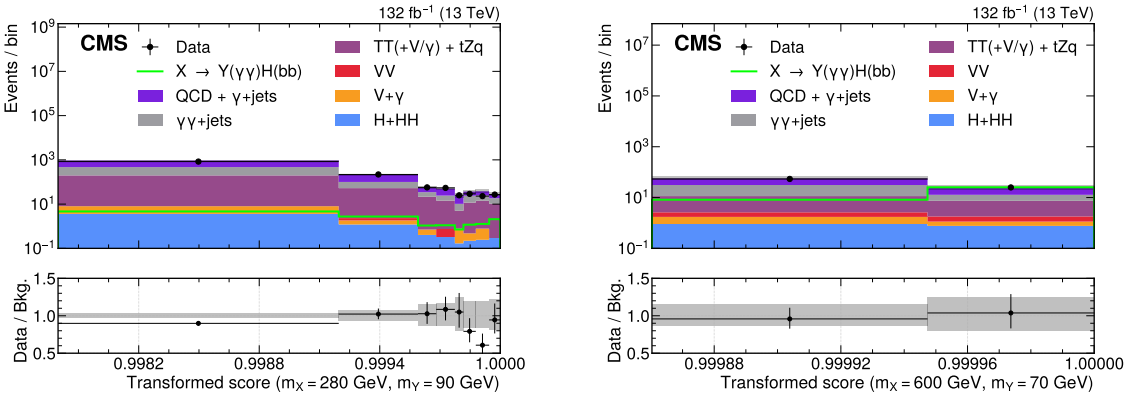

Figure 2. Distributions of the transformed PNN score for the signal hypotheses of $m_{\mathrm{X}} = 280\,\mathrm{GeV}$, $m_{\mathrm{Y}} = 90\,\mathrm{GeV}$ (left) and $m_{\mathrm{X}} = 600\,\mathrm{GeV}$, $m_{\mathrm{Y}} = 70\,\mathrm{GeV}$ (right) in their corresponding SRs. The bin boundaries correspond to the SR boundaries of each mass point, and the evolution of significance with transformed PNN score is shown: for bins with approximately the same background, the signal yield decreases towards the left (less sensitive categories), while the signal yield increases only when the background yield increases as well. The distributions are inclusive in the $m_{\gamma\gamma}$ distribution. The gray bands in the lower panels show the statistical uncertainty in the background estimation.

still slightly worse. In summary, the PNN brings a small performance gain to the analysis with respect to a simpler BDT classification while also providing the unique feature of using a single training to optimally probe multiple mass points, including those never used in training.

4.4 Event categorization

The PNN transformed score is used in the final event selection to define the SRs of the search. The SR boundaries are chosen to optimize the expected upper limit on the $\mathrm{X} \to \mathrm{Y}(\gamma\gamma)\mathrm{H}(\mathrm{b\bar{b}})$ cross section based on a simplified signal and background modeling. For illustration, the transformed score distributions in the SRs of the signal hypotheses of $(m_{\mathrm{X}}, m_{\mathrm{Y}}) = (280, 90)\,\mathrm{GeV}$ and $(m_{\mathrm{X}}, m_{\mathrm{Y}}) = (600, 70)\,\mathrm{GeV}$ are shown in figure 2. The details of the optimization procedure are given below. This method of optimization produced similar results to that of a method based on optimization of the significance.

First, the signal yields are extracted from the simulation in a ± 1 standard deviation window around the signal $m_{\gamma\gamma}$ peak, and the expected background yields within the same window are extracted from an exponential fit to data in a sideband region, i.e., the $m_{\gamma\gamma}$ distribution excluding a region $\pm 10\,\mathrm{GeV} m_{\mathrm{Y}}/m_{\mathrm{H}}$ around the signal peak, corresponding to the $m_{\gamma\gamma}$ resolution. Next, a constraint is placed on the minimum number of events required in the $m_{\gamma\gamma}$ sidebands in an SR. Initially, a minimum number of $N_{\mathrm{min}} = 20$ events is required, ensuring enough statistical power to perform the $m_{\gamma\gamma}$ sideband fits. The SR boundaries are defined as follows:

1. The first boundary is set at the value of the PNN transformed score which yields $N = N_{\mathrm{min}}$ events with scores higher than the boundary. We then compute for this SR the simplified expected upper limit, defined above, on the $\mathrm{X} \to \mathrm{Y}(\gamma\gamma)\mathrm{H}(\mathrm{b\bar{b}})$ cross section.

JHEP12(2025)178

2. Next, a new SR with the next N highest scoring events is considered, and the simplified expected limit is recomputed, based on the combination of the SRs.

3. If the addition of a new SR improves the simplified expected limit by at least 5%, then the new SR is incorporated and Step 2 is repeated for the next SR. Otherwise, this SR is not added and a new SR is formed with twice the number of highest scoring events ($N \to 2N$), and step 2 is repeated. The new value of N holds for all subsequent SRs as well.

This procedure continues until the number of events to be added in an SR is larger than the number of preselected events available, i.e., not having been assigned to a previous SR yet. A different number of SRs is created at different mass points: mass points with higher m_{X}-m_{Y} differences tend to have only a few SRs, while mass points with smaller m_{X}-m_{Y} differences can have up to around 10 SRs. The last region defined in this procedure has only a small contribution of potential signal and the highest background. As a result, it is considered as a control region (CR) for the purposes of background estimation, as discussed in section 5.2.

5 Signal and background modeling

In this section we describe the signal and backgrounds PDFs in the extended maximum likelihood fit of the $m_{\gamma\gamma}$ variable, used to extract the signal cross section, simultaneously across all SRs of a given signal mass hypothesis. To allow for the different m_{Y} hypotheses, PDFs are defined in a range of $65\,\mathrm{GeV} < m_{\gamma\gamma} < 1000\,\mathrm{GeV}$. Depending on the value of m_{Y}, data sidebands for nonresonant background fits are constructed around a "blinding region" defined as:

$$m_{\mathrm{Y}} \pm 10\,\mathrm{GeV}\frac{m_{\mathrm{Y}}}{m_{\mathrm{H}}} \tag{5.1}$$

5.1 Signal modeling

The $m_{\gamma\gamma}$ PDF for signal is taken from simulated signal events after the PNN selection has been applied, independently for each SR and for each year of data taking, since different data-taking periods exhibit up to 10% difference in the $m_{\gamma\gamma}$ resolution. Selected MC signal events consist predominantly of pairs of photons in the barrel part of the detector. As a result, the resolution for the $m_{\gamma\gamma}$ peak is driven by the photon resolution in the barrel, and further splitting the events in detector regions does not have an impact on the final result. For modeling the signal we use double Crystal-Ball (DCB) functions [65, 66]. Figure 3 shows simulated data fitted with DCB functions for two different mass hypotheses.

5.2 Background modeling

Background events are subdivided according to their different $m_{\gamma\gamma}$ PDFs: the continuum background arising from nonresonant diphoton events is described by a smoothly falling distribution in $m_{\gamma\gamma}$, while other background components peak in $m_{\gamma\gamma}$ (resonant backgrounds).

The $\mathrm{H} \to \gamma\gamma$ contribution, from both single H and double H production, is modeled using the same procedure used for signal events. Hence, their parametric models are very similar to the ones shown in figure 3 for the signal. The normalization of the different PDFs

JHEP12(2025)178

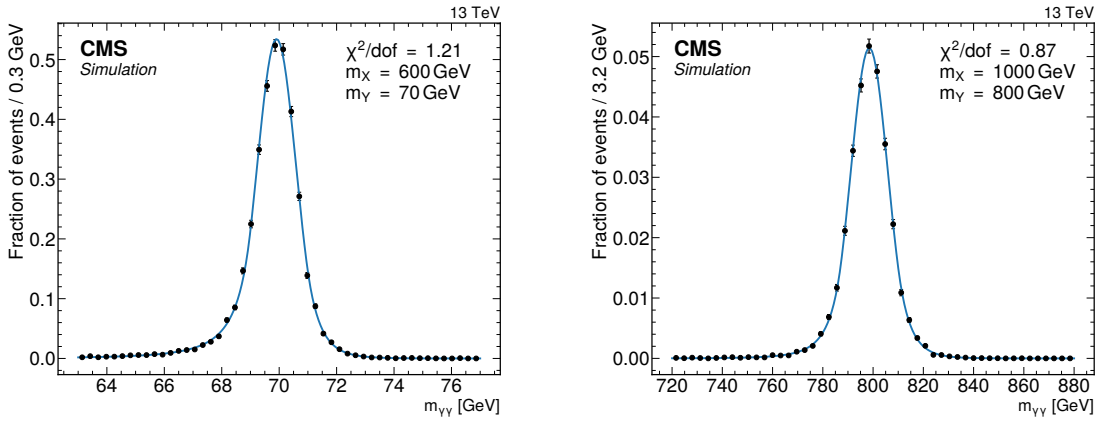

Figure 3. Parametric models of the signal process for $m_X = 600\,\text{GeV}$, $m_Y = 70\,\text{GeV}$ (left), and for $m_X = 1000\,\text{GeV}$, $m_Y = 800\,\text{GeV}$ (right) in their most sensitive SR. The histograms are normalized to unity. The acronym "dof" stands for the number of degrees of freedom of the parametric model.

is constrained to the best available cross section and branching fraction recommendations from the LHC Higgs Working Group [48].

A second resonant background contribution consists of DY events when the two electrons from a Z boson decay are misidentified as photons, resulting in a peak in the $m_{\gamma\gamma}$ spectrum close to the Z boson mass. This background is especially important for m_Y hypotheses around the Z mass, since this contribution can be mistakenly ascribed to a signal, if not properly accounted for.

We use a matrix ("ABCD") method, similar to the one described in ref. [67], to model this background. The procedure exploits the electron veto and the PNN output score variables, which are uncorrelated, and is based on three independent CRs in data, as described below:

- Region A is defined by inverting both the electron veto and the minimum PNN selection;
- Regions B are defined by inverting the electron veto. Multiple regions are defined as each one corresponds to one of the multiple signal regions of the analysis;
- Region C is defined by inverting the minimum PNN selection. This is the CR of the analysis, as defined in section 4.4;
- Regions D are the signal regions of the analysis.

By inverting the electron veto, regions A and B are enriched in DY events, with $Z \to e^+e^-$. Region B constrains the shape of the DY distribution in $m_{\gamma\gamma}$. The DY yields are extracted from regions A and C, thereby constraining the electron veto efficiency.

In all the regions, the target $Z \to e^+e^-$ process is isolated by a fitting procedure, with two components: one to model the peaking DY part, described in this paragraph, and one to model the continuum contribution, described in the next paragraph. The DY $m_{\gamma\gamma}$ PDFs are assumed to be the same in regions with the same PNN selection (in A and C, and in B and D). This assumption is justified by the fact that kinematic variables used by the PNN are

JHEP12(2025)178

not correlated with $m_{\gamma\gamma}$. For regions A and C, the PDF is modeled by a Gaussian function, except in cases where a poor goodness-of-fit is found and a DCB function is used instead. The rates of DY in regions A, B and C are included as free parameters in the maximum likelihood fit. The rate of the DY background in region D is given by the rate in region B, multiplied by the electron veto efficiency (rate in region C divided by rate in region A). The ABCD method is applied independently to each SR. Since the number of SRs depends on the m_{X} and m_{Y} hypothesis being considered, this implies the definition of a varying number of sub-regions B_i and D_i for each tested hypothesis, while in all cases, regions A and C are uniquely defined.

The procedure for selecting the candidate functions for modeling the $m_{\gamma\gamma}$ distribution of the continuum background is described below. The candidate PDFs, extracted separately in each SR of the analysis, are chosen from a set of different analytic functions (Bernstein polynomials, Laurent series, exponentials, and power laws). For each function type, we determine the minimum and maximum order of parameters by imposing a threshold on the goodness of fit to data and an $\mathcal{F}$-test [68], respectively. In the $\mathcal{F}$-test, each function is fit to the $m_{\gamma\gamma}$ distribution by minimizing the double negative logarithm of the likelihood ($-2\ln L$). To avoid biasing the background model with the eventual signal, fits to the data are performed in $m_{\gamma\gamma}$ sidebands. The size of the $m_{\gamma\gamma}$ SR depends on m_{Y} following the relation reported in eq. (5.1). In the fits, the normalization and the function parameters are included as freely floating parameters. We add a penalty term to the $-2\ln L$ which is proportional to the number of function parameters, with the goal to give preference to simple functions over more complex ones. Finally, we use the discrete profiling procedure [69] to take into account the systematic uncertainty associated with the choice of the functional form. In this procedure, a discrete nuisance parameter is associated with the choice of the function. This nuisance parameter is then profiled in a manner similar to the profiling of the other, continuous, nuisance parameters during the extended maximum likelihood fit of all regions relevant to a specific mass hypothesis. The potential bias of the nonresonant background estimation arising from a contribution from other signal mass hypotheses outside of the blinding region has been quantified to be of order 1% and is covered by this uncertainty.

As an illustration of the different components of our background estimation (continuum background from nonresonant processes and the Z and H resonances), in figure 4 we show the background-only fit and signal+background fit for $m_{\mathrm{X}} = 280\,\mathrm{GeV}$, $m_{\mathrm{Y}} = 90\,\mathrm{GeV}$ hypotheses in the two most sensitive SRs for this mass point.

6 Systematic uncertainties

The sensitivity of the search is driven by the integrated luminosity of the data set and the small number of events in the SRs. We do, however, account for a comprehensive set of systematic uncertainties, as described in this section.

The systematic uncertainties affecting the simulated samples used in the analysis (signal and Higgs production) are incorporated into the final maximum likelihood fit as nuisance parameters (NPs), and are described in detail below. The majority of these systematic uncertainties affect the overall expected event yields for both the signal and the single Higgs production. These uncertainties are modeled with log-normal probability distribution functions. For these processes there are also uncertainties in the measurements of the photon

JHEP12(2025)178

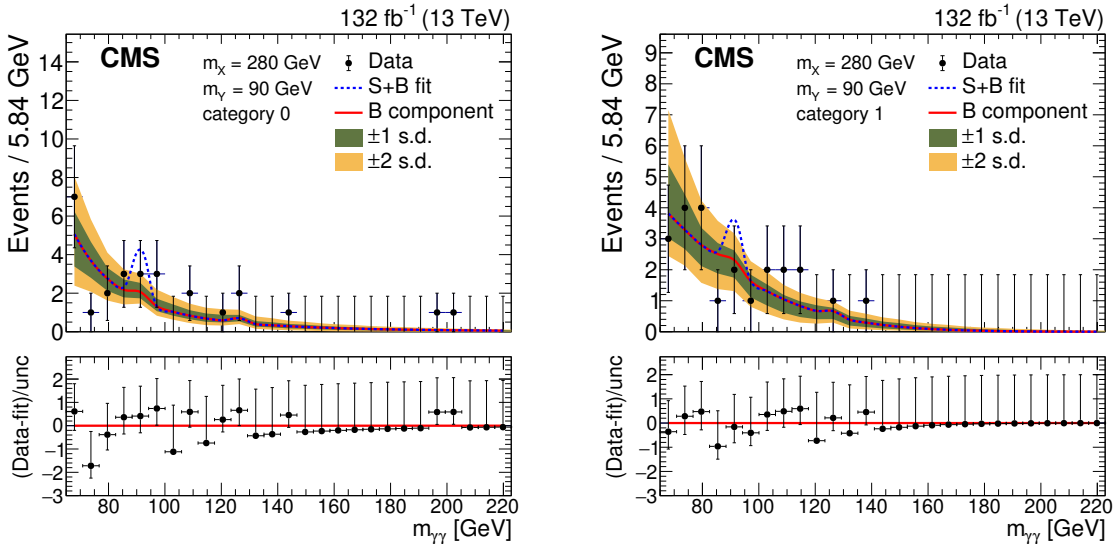

Figure 4. Background-only fit (solid red line) and signal+background fit (dashed blue line) for the mass point hypothesis of $m_{\mathrm{X}} = 280\,\mathrm{GeV}$, $m_{\mathrm{Y}} = 90\,\mathrm{GeV}$, shown for the most sensitive SR (left) and the second most sensitive SR (right). The points in the lower panel show the difference between the data and the background-only fit, divided by the average uncertainty in the data. The red line in the lower panel shows the background-only fit, which is by definition zero, and it is added as a visual aid. From left to right, the first and second most sensitive SRs are shown. The choice of the background functional form is determined by the maximum likelihood fit.

energies. These uncertainties impact the shape of the corresponding $m_{\gamma\gamma}$ distributions, and they are incorporated as NPs on the mean and the width of the $m_{\gamma\gamma}$ PDFs.

As discussed in section 5.2, the systematic uncertainty associated with the nonresonant background modeling is taken into account using the discrete profiling method. Finally, we use uniform priors for the transfer factors that determine the normalization of the resonant DY background.

6.1 Theoretical uncertainties

A number of theoretical uncertainties affect the normalization of the single and pair SM Higgs boson production processes:

- Theoretical uncertainties in the HH cross section:
  - The parton distribution functions, and the value of the strong force coupling constant (α_s), are estimated within the Born-improved approximation based on the PDF4LHC15nnlomc set [70]. They are found to be ±3.0%.
  - Uncertainties arising from the choice of the renormalization scheme and the scale of the top quark mass, and their combination with renormalization, μ_{R} and factorization, μ_{F}, scale variations are based on ref. [71]. They are found to be $^{+6\%}_{-23\%}$.
- Theoretical uncertainties in the single H boson production cross section:

JHEP12(2025)178

– QCD μ_R and μ_F scale variation values are taken following the recommendations of ref. [48], and typically result in an uncertainty of the order of 5–10%.

– The α_s variations are handled following the recommendations of ref. [70] and result in an up to 2% uncertainty in the cross section.

– The uncertainty associated with the parton distribution functions is computed following the PDF4LHC prescription [70, 72], and is typically of the order of 1%.

Finally, we consider the uncertainties in the branching fraction $\mathcal{B}(H \to \gamma\gamma)$ for both the single and double SM H processes. These are taken from ref. [48] and are estimated to be around 2%.

6.2 Experimental uncertainties

The experimental uncertainties that affect the normalization of the simulated signal and Higgs production samples are:

- Integrated luminosity: the integrated luminosities for the 2016, 2017, and 2018 data-taking years have 1.2–2.5% individual uncertainties [73–75], while the overall uncertainty for the 2016–2018 period is 1.6%. Since the signal and resonant H background fits are performed separately for the three data-taking periods, we use the year-dependent uncertainties and their correlations.

- Pileup: the uncertainties derived from the reweighting procedure to match the simulated pileup distribution to the one in the data, and originating from the variation of the minimum bias cross section [76], lead to an impact on the final results of less than 1%.

- Trigger: trigger efficiencies are measured with $Z \to e^+e^-$ data using the "tag-and-probe" method [77]. Their uncertainties are propagated throughout the analysis, including those associated with a small loss of efficiency due to a gradual shift in the ECAL trigger timing during the 2016 and 2017 data-taking periods. The size of the trigger-related uncertainties combined is less than 1%.

- Photon and diphoton identification: these uncertainties affect the final result at the 2% level.

- Jet energy correction (JEC) and jet energy resolution (JER): eleven separate sources of JEC uncertainties, as well as the uncertainty arising from the JERs, are propagated separately to the properties of jets in simulation [39]. These result in 12 systematic variations per year, which are propagated into the final result. The maximum impact of these uncertainties ranges between 0.7% and 3.0%, depending on the signal mass point.

- b tagging: the DeepJet output score is reshaped to correct for the differences between data and simulation [78]. The corresponding uncertainty sources involved in this procedure are included in the analysis, taking into account the appropriate correlation scheme. Nine separate sources of uncertainty are considered. We find the impact of these uncertainties to be less than 1% for each uncertainty source.

JHEP12(2025)178

The experimental uncertainties, affecting the shape of the $m_{\gamma\gamma}$ distribution, are evaluated with the "tag-and-probe" method with $Z \to e^+e^-$ data [77]. These uncertainties are:

- Photon energy scale and resolution: corrections are applied to simulation to match its photon energy scale and resolution to that of data. The size of these uncertainties combined is less than 1%.
- Tracker and ECAL material uncertainties: electrons showers tend to develop earlier than those of photons in the material of the tracker. Light collection efficiency differs for electrons and photons along the length of the ECAL crystals, and this leads to different ECAL responses. The uncertainty in the responses arising from these two effects is considered in the analysis, leading to an impact on the final results of approximately 1%.

As already mentioned at the beginning of the section, the sensitivity is dominated by the statistical uncertainties. The statistical uncertainty ranges from 30–50%, depending on the mass point, and the inclusion of all the systematic uncertainties increases the total uncertainty by up to 2% in absolute terms.

7 Results

The data are found to be compatible with the background-only expectation for most mass hypotheses probed in this search. We therefore extract upper limits on the process $X \to Y(\gamma\gamma)H(b\bar{b})$. The most significant deviation from the background-only hypothesis is discussed below.

The results quoted in this section have been determined using the CMS statistical analysis tool Combine [79], which is based on the RooFit [80] and RooStats [81] frameworks. Figure 5 shows the summary of expected and observed upper limits on the product, $\sigma\mathcal{B}$, of the signal cross section and the corresponding $\mathcal{B}$ to the final state particles for the different m_X and m_Y values considered in the analysis. Figure 6 illustrates the same expected and observed upper limits for the lowest and the highest sets of m_X mass points. While extracting results, both "nominal" mass points, i.e., the mass points on whose signal simulation the PNN has been trained, and "interpolated" mass points, i.e., mass points for which there is no simulation available, have been used. All of the results have been derived using the signal and background modeling methods described in detail in section 5. Systematic uncertainties are applied according to their description in section 6.

To achieve a sensitivity on the interpolated mass points comparable to that of the nominal mass points, we have leveraged the interpolating capabilities of the PNN. A dedicated PNN output is produced for each mass point that is used for the event categorization and the extraction of the results for the different signal hypotheses. Selected according to the dedicated PNN outputs, the data and the background simulation are used to extract the background models for the interpolated mass points, as described in section 5.2, while, in the absence of signal simulation for those mass points, the signal model parameters are interpolated between nominal mass points using linear splines. The interpolated mass points have been inserted at intervals corresponding to approximately twice the resolution at the given $m_{\gamma\gamma}$ range, i.e., ranging from 1 GeV up to 8 GeV.

JHEP12(2025)178

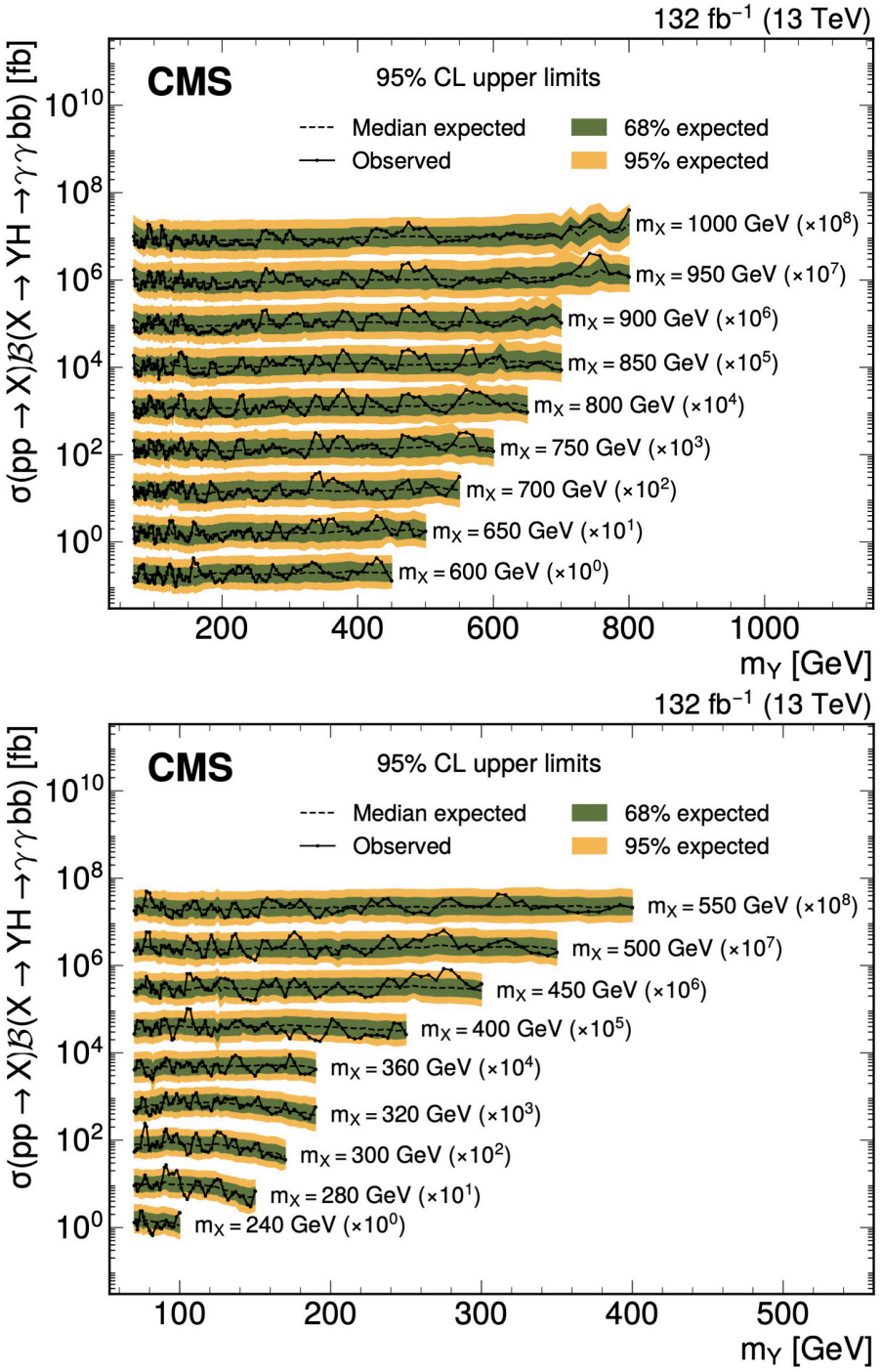

Figure 5. Observed (expected) upper limits on $\sigma\mathcal{B}$ for the $X \to Y(\gamma\gamma)H(b\bar{b})$ signal with the different mass hypotheses are shown with solid (dashed) lines, for mass points with m_X ranging from 600 to 1000 GeV (upper) and from 240 to 550 GeV (lower). The green and the yellow bands define the ±68% and ±95% uncertainty bands, respectively. For visualization purposes, the upper limits for mass points with different m_X have been multiplied with a constant factor quoted on the right of each band.

JHEP12(2025)178

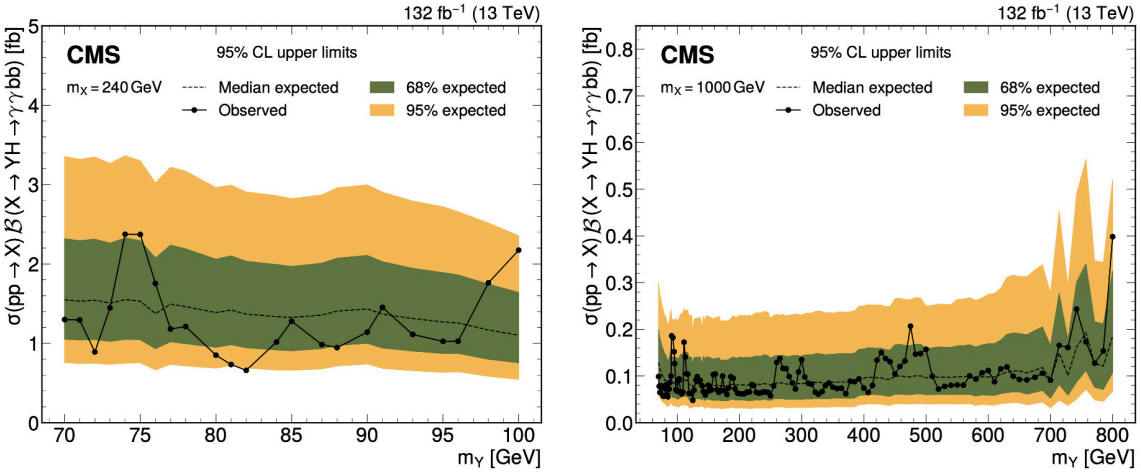

Figure 6. Observed (expected) upper limits on $\sigma\mathcal{B}$ for the $X \to Y(\gamma\gamma)H(b\bar{b})$ signal with the different m_Y hypotheses are shown with solid (dashed) lines, shown for the lowest $m_X = 240\,\text{GeV}$ (left) and for the highest $m_X = 1000\,\text{GeV}$ (right). The inner (green) band and the outer (yellow) band indicate the regions containing 68% and 95%, respectively, of the distribution of limits expected under the background-only hypothesis.

For a fixed m_X value, the limits tend to be weaker for low m_Y values ($m_Y < 200\,\text{GeV}$) owing to the larger backgrounds in that phase space region, and the presence of SM resonances. At higher m_Y values, the limits increase for mass points with lower $m_X - m_Y$ difference. This is attributed to the lower efficiency in distinguishing signal from background events in this phase space region. In contrast, for mass points with higher $m_X - m_Y$ difference, the observed limits are generally lower, reflecting the improved signal-to-background ratio. This behavior is a direct consequence of the different kinematic regions explored.

This is the first time that the $X \to Y(\gamma\gamma)H(b\bar{b})$ process is probed, i.e., with the resonance Y, which is of unknown mass, decaying to a photon pair. Given that the diphoton mass peak is usually exploited to tag the signal in similar final states, a moving signal peak poses additional experimental challenges. Despite these, the results of this analysis in terms of upper limits are comparable with those reported in the search for $X \to Y(b\bar{b})H(\gamma\gamma)$ [21].

In a recent $X \to Y(b\bar{b})H(\gamma\gamma)$ search, there was a local (global) excess of significance of 3.8 (2.6) standard deviations at $m_X = 650\,\text{GeV}$ and $m_Y = 90\,\text{GeV}$. However, in the current analysis, the observed limit at $m_X = 650\,\text{GeV}$ and $m_Y = 90\,\text{GeV}$ is in agreement with the SM, falling within 1 standard deviation of the median expected value. Under the assumption that the branching fractions of the Y to photons and b quarks are the same as the ones of the Higgs boson, as in the TRSM, the observed upper limit on $\sigma\mathcal{B}$ is 0.13 fb, which is compatible within two standard deviations with the best fit value of the excess of the $X \to Y(b\bar{b})H(\gamma\gamma)$ analysis at the same mass point, which was measured to be $0.35\,^{+0.17}_{-0.13}$ fb. Thus the results of this analysis do not confirm the excess.

In general, the data are found to be compatible with the SM expectation. A local significance of 3.33 standard deviations has been observed for the most significant deviation from the background-only hypothesis, at a mass point where the X and Y particles have a mass of 300 GeV and 77 GeV, respectively. Taking into account the large number (1699) of

JHEP12(2025)178

interpolated mass points probed in estimating the look-elsewhere effect [82], which refers to the probability of observing a fluctuation of equal or greater significance anywhere in the scanned (m_X,m_Y) mass plane, the global significance decreases to 0.65 standard deviations.

8 Summary

A search has been presented for the production of a new scalar resonance, X, decaying to a standard model Higgs boson and a new scalar resonance, Y, with the final state including a $b\bar{b}$ pair from the Higgs boson decay and a pair of photons from the Y particle decay. This search is the first targeting this final state combination. The analysis probes the mass range 240–1000 GeV for the resonance X and 70–800 GeV for the particle Y, and uses proton-proton collision data collected by the CMS experiment at $\sqrt{s} = 13$ TeV, corresponding to an integrated luminosity of 132 fb^{-1}.

In general, the data are found to be compatible with the background-only expectation. As a result, upper limits on the product of the production cross section of X and the branching fraction to the $b\bar{b}\gamma\gamma$ final state are derived at 95% confidence level as functions of the masses of the X and the Y particles. The observed (expected) upper limits are found to be between 0.05–2.69 (0.08–1.94) fb, depending on the assumed specific signal masses. A local (global) significance of 3.33 (0.65) standard deviations is observed for the most significant deviation from the background-only hypothesis, corresponding to $m_X = 300$ GeV and $m_Y = 77$ GeV.

Acknowledgments

We congratulate our colleagues in the CERN accelerator departments for the excellent performance of the LHC and thank the technical and administrative staffs at CERN and at other CMS institutes for their contributions to the success of the CMS effort. In addition, we gratefully acknowledge the computing centres and personnel of the Worldwide LHC Computing Grid and other centres for delivering so effectively the computing infrastructure essential to our analyses. Finally, we acknowledge the enduring support for the construction and operation of the LHC, the CMS detector, and the supporting computing infrastructure provided by the following funding agencies: SC (Armenia), BMBWF and FWF (Austria); FNRS and FWO (Belgium); CNPq, CAPES, FAPERJ, FAPERGS, and FAPESP (Brazil); MES and BNSF (Bulgaria); CERN; CAS, MoST, and NSFC (China); MINCIENCIAS (Colombia); MSES and CSF (Croatia); RIF (Cyprus); SENESCYT (Ecuador); ERC PRG, TARISTU24-TK10 and MoER TK202 (Estonia); Academy of Finland, MEC, and HIP (Finland); CEA and CNRS/IN2P3 (France); SRNSF (Georgia); BMBF, DFG, and HGF (Germany); GSRI (Greece); NKFIH (Hungary); DAE and DST (India); IPM (Iran); SFI (Ireland); INFN (Italy); MSIT and NRF (Republic of Korea); MES (Latvia); LMTLT (Lithuania); MOE and UM (Malaysia); BUAP, CINVESTAV, CONACYT, LNS, SEP, and UASLP-FAI (Mexico); MOS (Montenegro); MBIE (New Zealand); PAEC (Pakistan); MES, NSC, and NAWA (Poland); FCT (Portugal); MESTD (Serbia); MICIU/AEI and PCTI (Spain); MOSTR (Sri Lanka); Swiss Funding Agencies (Switzerland); MST (Taipei); MHESI and NSTDA (Thailand); TUBITAK and TENMAK (Türkiye); NASU (Ukraine); STFC (United Kingdom); DOE and NSF (U.S.A.).

JHEP12(2025)178

Individuals have received support from the Marie-Curie programme and the European Research Council and Horizon 2020 Grant, contract Nos. 675440, 724704, 752730, 758316, 765710, 824093, 101115353, 101002207, 101001205, and COST Action CA16108 (European Union); the Leventis Foundation; the Alfred P. Sloan Foundation; the Alexander von Humboldt Foundation; the Science Committee, project no. 22rl-037 (Armenia); the Fonds pour la Formation à la Recherche dans l'Industrie et dans l'Agriculture (FRIA-Belgium); the Beijing Municipal Science & Technology Commission, No. Z191100007219010, the Fundamental Research Funds for the Central Universities, the Ministry of Science and Technology of China under Grant No. 2023YFA1605804, and the Natural Science Foundation of China under Grant No. 12061141002 (China); the Ministry of Education, Youth and Sports (MEYS) of the Czech Republic; the Shota Rustaveli National Science Foundation, grant FR-22-985 (Georgia); the Deutsche Forschungsgemeinschaft (DFG), among others, under Germany's Excellence Strategy — EXC 2121 "Quantum Universe" — 390833306, and under project number 400140256 — GRK2497; the Hellenic Foundation for Research and Innovation (HFRI), Project Number 2288 (Greece); the Hungarian Academy of Sciences, the New National Excellence Program — ÚNKP, the NKFIH research grants K 131991, K 133046, K 138136, K 143460, K 143477, K 146913, K 146914, K 147048, 2020-2.2.1-ED-2021-00181, TKP2021-NKTA-64, and 2021-4.1.2-NEMZ_KI-2024-00036 (Hungary); the Council of Science and Industrial Research, India; ICSC — National Research Centre for High Performance Computing, Big Data and Quantum Computing, FAIR — Future Artificial Intelligence Research, and CUP I53D23001070006 (Mission 4 Component 1), funded by the NextGenerationEU program (Italy); the Latvian Council of Science; the Ministry of Education and Science, project no. 2022/WK/14, and the National Science Center, contracts Opus 2021/41/B/ST2/01369, 2021/43/B/ST2/01552, 2023/49/B/ST2/03273, and the NAWA contract BPN/PPO/2021/1/00011 (Poland); the Fundação para a Ciência e a Tecnologia, grant CEECIND/01334/2018 (Portugal); the National Priorities Research Program by Qatar National Research Fund; MICIU/AEI/10.13039/501100011033, ERDF/EU, "European Union NextGenerationEU/PRTR", and Programa Severo Ochoa del Principado de Asturias (Spain); the Chulalongkorn Academic into Its 2nd Century Project Advancement Project, and the National Science, Research and Innovation Fund via the Program Management Unit for Human Resources & Institutional Development, Research and Innovation, grant B39G680009 (Thailand); the Kavli Foundation; the Nvidia Corporation; the SuperMicro Corporation; the Welch Foundation, contract C-1845; and the Weston Havens Foundation (U.S.A.).

Data Availability Statement. Release and preservation of data used by the CMS Collaboration as the basis for publications is guided by the CMS data preservation, re-use and open access policy.

Code Availability Statement. The CMS core software is publicly available on GitHub.

JHEP12(2025)178

References

[1] ATLAS collaboration, *Observation of a new particle in the search for the Standard Model Higgs boson with the ATLAS detector at the LHC*, *Phys. Lett. B* **716** (2012) 1 [arXiv:1207.7214] [INSPIRE].

[2] CMS collaboration, *Observation of a new boson at a mass of 125 GeV with the CMS experiment at the LHC*, *Phys. Lett. B* **716** (2012) 30 [arXiv:1207.7235] [INSPIRE].

[3] CMS collaboration, *Observation of a new boson with mass near 125 GeV in pp collisions at* $\sqrt{s} = 7$ *and* 8 *TeV*, *JHEP* **06** (2013) 081 [arXiv:1303.4571] [INSPIRE].

[4] ATLAS collaboration, *A detailed map of Higgs boson interactions by the ATLAS experiment ten years after the discovery*, *Nature* **607** (2022) 52 [*Erratum ibid.* **612** (2022) E24] [arXiv:2207.00092] [INSPIRE].

[5] CMS collaboration, *A portrait of the Higgs boson by the CMS experiment ten years after the discovery*, *Nature* **607** (2022) 60 [arXiv:2207.00043] [INSPIRE].

[6] P. Ramond, *Dual theory for free fermions*, *Phys. Rev. D* **3** (1971) 2415 [INSPIRE].

[7] Y.A. Golfand and E.P. Likhtman, *Extension of the algebra of Poincaré group generators and violation of p invariance*, *JETP Lett.* **13** (1971) 323 [INSPIRE].

[8] A. Neveu and J.H. Schwarz, *Factorizable dual model of pions*, *Nucl. Phys. B* **31** (1971) 86 [INSPIRE].

[9] D.V. Volkov and V.P. Akulov, *Possible universal neutrino interaction*, *JETP Lett.* **16** (1972) 438 [INSPIRE].

[10] J. Wess and B. Zumino, *A Lagrangian model invariant under supergauge transformations*, *Phys. Lett. B* **49** (1974) 52 [INSPIRE].

[11] J. Wess and B. Zumino, *Supergauge transformations in four-dimensions*, *Nucl. Phys. B* **70** (1974) 39 [INSPIRE].

[12] P. Fayet, *Supergauge invariant extension of the Higgs mechanism and a model for the electron and its neutrino*, *Nucl. Phys. B* **90** (1975) 104 [INSPIRE].

[13] H.P. Nilles, *Supersymmetry, supergravity and particle physics*, *Phys. Rept.* **110** (1984) 1 [INSPIRE].

[14] MSSM Working Group collaboration, *The minimal supersymmetric standard model: group summary report*, in the proceedings of the *GDR (Groupement De Recherche) — Supersymetrie*, Montpellier, France, 15–17 April 1998 [hep-ph/9901246] [INSPIRE].

[15] U. Ellwanger, C. Hugonie and A.M. Teixeira, *The next-to-minimal supersymmetric standard model*, *Phys. Rept.* **496** (2010) 1 [arXiv:0910.1785] [INSPIRE].

[16] T. Robens, T. Stefaniak and J. Wittbrodt, *Two-real-scalar-singlet extension of the SM: LHC phenomenology and benchmark scenarios*, *Eur. Phys. J. C* **80** (2020) 151 [arXiv:1908.08554] [INSPIRE].

[17] H. Abouabid et al., *Benchmarking di-Higgs production in various extended Higgs sector models*, *JHEP* **09** (2022) 011 [arXiv:2112.12515] [INSPIRE].

[18] CMS collaboration, *Search for a massive scalar resonance decaying to a light scalar and a Higgs boson in the four b quarks final state with boosted topology*, *Phys. Lett. B* **842** (2023) 137392 [arXiv:2204.12413] [INSPIRE].

JHEP12(2025)178

[19] CMS collaboration, *Search for a heavy Higgs boson decaying into two lighter Higgs bosons in the $\tau\tau bb$ final state at 13 TeV*, *JHEP* **11** (2021) 057 [arXiv:2106.10361] [INSPIRE].

[20] CMS collaboration, *Search for the nonresonant and resonant production of a Higgs boson in association with an additional scalar boson in the $\gamma\gamma\tau\tau$ final state in proton-proton collisions at $\sqrt{s} = 13$ TeV*, arXiv:2506.23012 [INSPIRE].

[21] CMS collaboration, *Search for a new resonance decaying into two spin-0 bosons in a final state with two photons and two bottom quarks in proton-proton collisions at $\sqrt{s} = 13$ TeV*, *JHEP* **05** (2024) 316 [arXiv:2310.01643] [INSPIRE].

[22] CMS collaboration, *Search for a standard model-like Higgs boson in the mass range between 70 and 110 GeV in the diphoton final state in proton-proton collisions at $\sqrt{s} = 13$ TeV*, *Phys. Lett. B* **860** (2025) 139067 [arXiv:2405.18149] [INSPIRE].

[23] *HEPData record for this analysis*, https://doi.org/10.17182/hepdata.158364 (2025).

[24] CMS collaboration, *The CMS experiment at the CERN LHC*, 2008 *JINST* **3** S08004 [INSPIRE].

[25] CMS collaboration, *Development of the CMS detector for the CERN LHC run 3*, 2024 *JINST* **19** P05064 [arXiv:2309.05466] [INSPIRE].

[26] CMS collaboration, *Performance of the CMS level-1 trigger in proton-proton collisions at $\sqrt{s} = 13$ TeV*, 2020 *JINST* **15** P10017 [arXiv:2006.10165] [INSPIRE].

[27] CMS collaboration, *The CMS trigger system*, 2017 *JINST* **12** P01020 [arXiv:1609.02366] [INSPIRE].

[28] CMS collaboration, *Performance of the CMS high-level trigger during LHC run 2*, 2024 *JINST* **19** P11021 [arXiv:2410.17038] [INSPIRE].

[29] D. Contardo et al., *Technical proposal for the phase-II upgrade of the CMS detector*, CERN-LHCC-2015-010, CERN, Geneva, Switzerland (2015) [DOI:10.17181/CERN.VU8I.D59J] [INSPIRE].

[30] CMS collaboration, *Particle-flow reconstruction and global event description with the CMS detector*, 2017 *JINST* **12** P10003 [arXiv:1706.04965] [INSPIRE].

[31] CMS collaboration, *Performance of photon reconstruction and identification with the CMS detector in proton-proton collisions at $\sqrt{s} = 8$ TeV*, 2015 *JINST* **10** P08010 [arXiv:1502.02702] [INSPIRE].

[32] CMS collaboration, *A measurement of the Higgs boson mass in the diphoton decay channel*, *Phys. Lett. B* **805** (2020) 135425 [arXiv:2002.06398] [INSPIRE].

[33] CMS collaboration, *Electron and photon reconstruction and identification with the CMS experiment at the CERN LHC*, 2021 *JINST* **16** P05014 [arXiv:2012.06888] [INSPIRE].

[34] CMS collaboration, *ECAL 2016 refined calibration and run 2 summary plots*, CMS-DP-2020-021, CERN, Geneva, Switzerland (2020).

[35] CMS collaboration, *Performance of CMS muon reconstruction in pp collision events at $\sqrt{s} = 7$ TeV*, 2012 *JINST* **7** P10002 [arXiv:1206.4071] [INSPIRE].

[36] M. Cacciari, G.P. Salam and G. Soyez, *The anti-k_t jet clustering algorithm*, *JHEP* **04** (2008) 063 [arXiv:0802.1189] [INSPIRE].

[37] M. Cacciari, G.P. Salam and G. Soyez, *FastJet user manual*, *Eur. Phys. J. C* **72** (2012) 1896 [arXiv:1111.6097] [INSPIRE].

JHEP12(2025)178

[38] CMS collaboration, *Pileup mitigation at CMS in 13 TeV data*, 2020 *JINST* **15** P09018 [arXiv:2003.00503] [INSPIRE].

[39] CMS collaboration, *Jet energy scale and resolution in the CMS experiment in pp collisions at 8 TeV*, 2017 *JINST* **12** P02014 [arXiv:1607.03663] [INSPIRE].

[40] E. Bols et al., *Jet flavour classification using DeepJet*, 2020 *JINST* **15** P12012 [arXiv:2008.10519] [INSPIRE].

[41] CMS collaboration, *Performance of the DeepJet b tagging algorithm using 41.9 fb of data from proton-proton collisions at 13 TeV with phase 1 CMS detector*, CMS-DP-2018-058, CERN, Geneva, Switzerland (2018).

[42] CMS collaboration, *Event generator tunes obtained from underlying event and multiparton scattering measurements*, *Eur. Phys. J. C* **76** (2016) 155 [arXiv:1512.00815] [INSPIRE].

[43] CMS collaboration, *Extraction and validation of a new set of CMS PYTHIA8 tunes from underlying-event measurements*, *Eur. Phys. J. C* **80** (2020) 4 [arXiv:1903.12179] [INSPIRE].

[44] NNPDF collaboration, *Parton distributions from high-precision collider data*, *Eur. Phys. J. C* **77** (2017) 663 [arXiv:1706.00428] [INSPIRE].

[45] GEANT4 collaboration, *GEANT4 — a simulation toolkit*, *Nucl. Instrum. Meth. A* **506** (2003) 250 [INSPIRE].

[46] J. Alwall et al., *The automated computation of tree-level and next-to-leading order differential cross sections, and their matching to parton shower simulations*, *JHEP* **07** (2014) 079 [arXiv:1405.0301] [INSPIRE].

[47] R. Frederix et al., *The automation of next-to-leading order electroweak calculations*, *JHEP* **11** (2018) 085 [*Erratum ibid.* **11** (2021) 085] [arXiv:1804.10017] [INSPIRE].

[48] LHC Higgs Cross Section Working Group collaboration, *Handbook of LHC Higgs cross sections: 4. Deciphering the nature of the Higgs sector*, *CERN Yellow Rep. Monogr.* **2** (2017) 1 [arXiv:1610.07922] [INSPIRE].

[49] S. Frixione, P. Nason and C. Oleari, *Matching NLO QCD computations with parton shower simulations: the POWHEG method*, *JHEP* **11** (2007) 070 [arXiv:0709.2092] [INSPIRE].

[50] S. Alioli, P. Nason, C. Oleari and E. Re, *NLO single-top production matched with shower in POWHEG: s- and t-channel contributions*, *JHEP* **09** (2009) 111 [*Erratum ibid.* **02** (2010) 011] [arXiv:0907.4076] [INSPIRE].

[51] T. Melia, P. Nason, R. Rontsch and G. Zanderighi, W^+W^-, WZ *and* ZZ *production in the POWHEG BOX*, *JHEP* **11** (2011) 078 [arXiv:1107.5051] [INSPIRE].

[52] P. Nason and G. Zanderighi, W^+W^- , WZ *and* ZZ *production in the POWHEG-BOX-V2*, *Eur. Phys. J. C* **74** (2014) 2702 [arXiv:1311.1365] [INSPIRE].

[53] E. Bagnaschi, G. Degrassi, P. Slavich and A. Vicini, *Higgs production via gluon fusion in the POWHEG approach in the SM and in the MSSM*, *JHEP* **02** (2012) 088 [arXiv:1111.2854] [INSPIRE].

[54] G. Heinrich, S.P. Jones, M. Kerner and L. Scyboz, *A non-linear EFT description of* $gg \to HH$ *at NLO interfaced to POWHEG*, *JHEP* **10** (2020) 021 [arXiv:2006.16877] [INSPIRE].

[55] G. Heinrich et al., *Probing the trilinear Higgs boson coupling in di-Higgs production at NLO QCD including parton shower effects*, *JHEP* **06** (2019) 066 [arXiv:1903.08137] [INSPIRE].

[56] S. Jones and S. Kuttimalai, *Parton shower and NLO-matching uncertainties in Higgs boson pair production*, *JHEP* **02** (2018) 176 [arXiv:1711.03319] [INSPIRE].

JHEP12(2025)178

[57] G. Heinrich et al., *NLO predictions for Higgs boson pair production with full top quark mass dependence matched to parton showers*, *JHEP* **08** (2017) 088 [arXiv:1703.09252] [INSPIRE].

[58] G. Buchalla et al., *Higgs boson pair production in non-linear effective field theory with full m_t-dependence at NLO QCD*, *JHEP* **09** (2018) 057 [*Erratum ibid.* **06** (2025) 094] [arXiv:1806.05162] [INSPIRE].

[59] T. Gleisberg et al., *Event generation with SHERPA 1.1*, *JHEP* **02** (2009) 007 [arXiv:0811.4622] [INSPIRE].

[60] T. Sjöstrand et al., *An introduction to PYTHIA 8.2*, *Comput. Phys. Commun.* **191** (2015) 159 [arXiv:1410.3012] [INSPIRE].

[61] CMS collaboration, *Performance of the CMS muon detector and muon reconstruction with proton-proton collisions at $\sqrt{s} = 13$ TeV*, 2018 *JINST* **13** P06015 [arXiv:1804.04528] [INSPIRE].

[62] CMS collaboration, *Performance of missing transverse momentum reconstruction in proton-proton collisions at $\sqrt{s} = 13$ TeV using the CMS detector*, 2019 *JINST* **14** P07004 [arXiv:1903.06078] [INSPIRE].

[63] CMS collaboration, *Measurements of $t\bar{t}H$ production and the CP structure of the Yukawa interaction between the Higgs boson and top quark in the diphoton decay channel*, *Phys. Rev. Lett.* **125** (2020) 061801 [arXiv:2003.10866] [INSPIRE].

[64] P. Baldi et al., *Parameterized neural networks for high-energy physics*, *Eur. Phys. J. C* **76** (2016) 235 [arXiv:1601.07913] [INSPIRE].

[65] M. Oreglia, *A study of the reactions $\psi' \to \gamma\gamma\psi$*, Ph.D. thesis, Stanford University, Stanford, CA, U.S.A. (1980) [INSPIRE].

[66] J.E. Gaiser, *Charmonium spectroscopy from radiative decays of the J/ψ and ψ'*, Ph.D. thesis, Stanford University, Stanford, CA, U.S.A. (1982) [INSPIRE].

[67] S. Choi and H. Oh, *Improved extrapolation methods of data-driven background estimations in high energy physics*, *Eur. Phys. J. C* **81** (2021) 643 [arXiv:1906.10831] [INSPIRE].

[68] R.A. Fisher, *On the mathematical foundations of theoretical statistics*, *Phil. Trans. Roy. Soc. Lond. A* **222** (1922) 309 [INSPIRE].

[69] P.D. Dauncey, M. Kenzie, N. Wardle and G.J. Davies, *Handling uncertainties in background shapes: the discrete profiling method*, 2015 *JINST* **10** P04015 [arXiv:1408.6865] [INSPIRE].

[70] J. Butterworth et al., *PDF4LHC recommendations for LHC run II*, *J. Phys. G* **43** (2016) 023001 [arXiv:1510.03865] [INSPIRE].

[71] J. Baglio et al., *$gg \to HH$: combined uncertainties*, *Phys. Rev. D* **103** (2021) 056002 [arXiv:2008.11626] [INSPIRE].

[72] LHC Higgs Cross Section Working Group collaboration, *Handbook of LHC Higgs cross sections: 3. Higgs properties*, arXiv:1307.1347 [DOI:10.5170/CERN-2013-004] [INSPIRE].

[73] CMS collaboration, *Precision luminosity measurement in proton-proton collisions at $\sqrt{s} = 13$ TeV in 2015 and 2016 at CMS*, *Eur. Phys. J. C* **81** (2021) 800 [arXiv:2104.01927] [INSPIRE].

[74] CMS collaboration, *CMS luminosity measurement for the 2017 data-taking period at $\sqrt{s} = 13$ TeV*, CMS-PAS-LUM-17-004, CERN, Geneva, Switzerland (2018) [INSPIRE].

[75] CMS collaboration, *CMS luminosity measurement for the 2018 data-taking period at $\sqrt{s} = 13$ TeV*, CMS-PAS-LUM-18-002, CERN, Geneva, Swizerland (2019) [INSPIRE].

JHEP12(2025)178

[76] CMS collaboration, *Measurement of the inelastic proton-proton cross section at $\sqrt{s} = 13$ TeV*, *JHEP* **07** (2018) 161 [arXiv:1802.02613] [INSPIRE].

[77] CMS collaboration, *Measurement of the inclusive W and Z production cross sections in pp collisions at $\sqrt{s} = 7$ TeV*, *JHEP* **10** (2011) 132 [arXiv:1107.4789] [INSPIRE].

[78] CMS collaboration, *Identification of heavy-flavour jets with the CMS detector in pp collisions at 13 TeV*, 2018 *JINST* **13** P05011 [arXiv:1712.07158] [INSPIRE].

[79] CMS collaboration, *The CMS statistical analysis and combination tool: Combine*, *Comput. Softw. Big Sci.* **8** (2024) 19 [arXiv:2404.06614] [INSPIRE].

[80] W. Verkerke and D.P. Kirkby, *The RooFit toolkit for data modeling*, *eConf C* **0303241** (2003) MOLT007 [physics/0306116] [INSPIRE].

[81] L. Moneta et al., *The RooStats project*, *PoS* **ACAT2010** (2010) 057 [arXiv:1009.1003] [INSPIRE].

[82] E. Gross and O. Vitells, *Trial factors for the look elsewhere effect in high energy physics*, *Eur. Phys. J. C* **70** (2010) 525 [arXiv:1005.1891] [INSPIRE].

JHEP12(2025)178

The CMS collaboration

Yerevan Physics Institute, Yerevan, Armenia

A. Hayrapetyan, V. Makarenko, A. Tumasyan[1]

Institut für Hochenergiephysik, Vienna, Austria

W. Adam, J.W. Andrejkovic, L. Benato, T. Bergauer, M. Dragicevic, C. Giordano, P.S. Hussain, M. Jeitler[2], N. Krammer, A. Li, D. Liko, M. Matthewman, I. Mikulec, J. Schieck[2], R. Schöfbeck[2], D. Schwarz, M. Shooshtari, M. Sonawane, W. Waltenberger, C.-E. Wulz[2]

Universiteit Antwerpen, Antwerpen, Belgium

T. Janssen, H. Kwon, D. Ocampo Henao, T. Van Laer, P. Van Mechelen

Vrije Universiteit Brussel, Brussel, Belgium

J. Bierkens, N. Breugelmans, J. D'Hondt, S. Dansana, A. De Moor, M. Delcourt, F. Heyen, Y. Hong, P. Kashko, S. Lowette, I. Makarenko, D. Müller, J. Song, S. Tavernier, M. Tytgat[3], G.P. Van Onsem, S. Van Putte, D. Vannerom

Université Libre de Bruxelles, Bruxelles, Belgium

B. Bilin, B. Clerbaux, A.K. Das, I. De Bruyn, G. De Lentdecker, H. Evard, L. Favart, P. Gianneios, A. Khalilzadeh, F.A. Khan, A. Malara, M.A. Shahzad, L. Thomas, M. Vanden Bemden, C. Vander Velde, P. Vanlaer, F. Zhang

Ghent University, Ghent, Belgium

M. De Coen, D. Dobur, G. Gokbulut, J. Knolle, L. Lambrecht, D. Marckx, K. Skovpen, N. Van Den Bossche, J. van der Linden, J. Vandenbroeck, L. Wezenbeek

Université Catholique de Louvain, Louvain-la-Neuve, Belgium

S. Bein, A. Benecke, A. Bethani, G. Bruno, A. Cappati, J. De Favereau De Jeneret, C. Delaere, A. Giammanco, A.O. Guzel, V. Lemaitre, J. Lidrych, P. Malek, P. Mastrapasqua, S. Turkcapar

Centro Brasileiro de Pesquisas Fisicas, Rio de Janeiro, Brazil

G.A. Alves, M. Barroso Ferreira Filho, E. Coelho, C. Hensel, T. Menezes De Oliveira, C. Mora Herrera[4], P. Rebello Teles, M. Soeiro, E.J. Tonelli Manganote[5], A. Vilela Pereira[4]

Universidade do Estado do Rio de Janeiro, Rio de Janeiro, Brazil

W.L. Aldá Júnior, H. Brandao Malbouisson, W. Carvalho, J. Chinellato[6], M. Costa Reis, E.M. Da Costa, G.G. Da Silveira[7], D. De Jesus Damiao, S. Fonseca De Souza, R. Gomes De Souza, S. S. Jesus, T. Laux Kuhn[7], M. Macedo, K. Mota Amarilo, L. Mundim, H. Nogima, J.P. Pinheiro, A. Santoro, A. Sznajder, M. Thiel, F. Torres Da Silva De Araujo[8]

JHEP12(2025)178

Universidade Estadual Paulista, Universidade Federal do ABC, São Paulo, Brazil
C.A. Bernardes[7], T.R. Fernandez Perez Tomei, E.M. Gregores, B. Lopes Da Costa, I. Maietto Silverio, P.G. Mercadante, S.F. Novaes, B. Orzari, Sandra S. Padula, V. Scheurer

Institute for Nuclear Research and Nuclear Energy, Bulgarian Academy of Sciences, Sofia, Bulgaria
A. Aleksandrov, G. Antchev, P. Danev, R. Hadjiiska, P. Iaydjiev, M. Misheva, M. Shopova, G. Sultanov

University of Sofia, Sofia, Bulgaria
A. Dimitrov, L. Litov, B. Pavlov, P. Petkov, A. Petrov

Instituto De Alta Investigación, Universidad de Tarapacá, Casilla 7 D, Arica, Chile
S. Keshri, D. Laroze, S. Thakur

Universidad Tecnica Federico Santa Maria, Valparaiso, Chile
W. Brooks

Beihang University, Beijing, China
T. Cheng, T. Javaid, L. Wang, L. Yuan

Department of Physics, Tsinghua University, Beijing, China
Z. Hu, Z. Liang, J. Liu, X. Wang

Institute of High Energy Physics, Beijing, China
G.M. Chen[9], H.S. Chen[9], M. Chen[9], Y. Chen, Q. Hou, X. Hou, F. Iemmi, C.H. Jiang, A. Kapoor[10], H. Liao, G. Liu, Z.-A. Liu[11], J.N. Song[11], S. Song, J. Tao, C. Wang[9], J. Wang, H. Zhang, J. Zhao

State Key Laboratory of Nuclear Physics and Technology, Peking University, Beijing, China
A. Agapitos, Y. Ban, A. Carvalho Antunes De Oliveira, S. Deng, B. Guo, Q. Guo, C. Jiang, A. Levin, C. Li, Q. Li, Y. Mao, S. Qian, S.J. Qian, X. Qin, X. Sun, D. Wang, J. Wang, H. Yang, M. Zhang, Y. Zhao, C. Zhou

State Key Laboratory of Nuclear Physics and Technology, Institute of Quantum Matter, South China Normal University, Guangzhou, China
S. Yang

Sun Yat-Sen University, Guangzhou, China
Z. You

University of Science and Technology of China, Hefei, China
K. Jaffel, N. Lu

JHEP12(2025)178

Nanjing Normal University, Nanjing, China
G. Bauer[12,13], B. Li[14], H. Wang, K. Yi[15], J. Zhang

Institute of Modern Physics and Key Laboratory of Nuclear Physics and Ion-beam Application (MOE) — Fudan University, Shanghai, China
Y. Li

Zhejiang University, Hangzhou, Zhejiang, China
Z. Lin, C. Lu, M. Xiao[16]

Universidad de Los Andes, Bogota, Colombia
C. Avila, D.A. Barbosa Trujillo, A. Cabrera, C. Florez, J. Fraga, J.A. Reyes Vega

Universidad de Antioquia, Medellin, Colombia
C. Rendón, M. Rodriguez, A.A. Ruales Barbosa, J.D. Ruiz Alvarez

University of Split, Faculty of Electrical Engineering, Mechanical Engineering and Naval Architecture, Split, Croatia
N. Godinovic, D. Lelas, A. Sculac

University of Split, Faculty of Science, Split, Croatia
M. Kovac, A. Petkovic, T. Sculac

Institute Rudjer Boskovic, Zagreb, Croatia
P. Bargassa, V. Brigljevic, B.K. Chitroda, D. Ferencek, K. Jakovcic, A. Starodumov, T. Susa

University of Cyprus, Nicosia, Cyprus
A. Attikis, K. Christoforou, A. Hadjiagapiou, C. Leonidou, C. Nicolaou, L. Paizanos, F. Ptochos, P.A. Razis, H. Rykaczewski, H. Saka, A. Stepennov

Charles University, Prague, Czech Republic
M. Finger[†], M. Finger Jr.

Escuela Politecnica Nacional, Quito, Ecuador
E. Ayala

Universidad San Francisco de Quito, Quito, Ecuador
E. Carrera Jarrin

Academy of Scientific Research and Technology of the Arab Republic of Egypt, Egyptian Network of High Energy Physics, Cairo, Egypt
H. Abdalla[17], Y. Assran[18,19]

Center for High Energy Physics (CHEP-FU), Fayoum University, El-Fayoum, Egypt
M. Abdullah Al-Mashad, A. Hussein, H. Mohammed

JHEP12(2025)178

National Institute of Chemical Physics and Biophysics, Tallinn, Estonia
K. Ehataht, M. Kadastik, T. Lange, C. Nielsen, J. Pata, M. Raidal, N. Seeba, L. Tani

Department of Physics, University of Helsinki, Helsinki, Finland
A. Milieva, K. Osterberg, M. Voutilainen

Helsinki Institute of Physics, Helsinki, Finland
N. Bin Norjoharuddeen, E. Brücken, F. Garcia, P. Inkaew, K.T.S. Kallonen, R. Kumar Verma, T. Lampén, K. Lassila-Perini, B. Lehtela, S. Lehti, T. Lindén, N.R. Mancilla Xinto, M. Myllymäki, M.m. Rantanen, S. Saariokari, N.T. Toikka, J. Tuominiemi

Lappeenranta-Lahti University of Technology, Lappeenranta, Finland
H. Kirschenmann, P. Luukka, H. Petrow

IRFU, CEA, Université Paris-Saclay, Gif-sur-Yvette, France
M. Besancon, F. Couderc, M. Dejardin, D. Denegri, P. Devouge, J.L. Faure, F. Ferri, P. Gaigne, S. Ganjour, P. Gras, G. Hamel de Monchenault, M. Kumar, V. Lohezic, J. Malcles, F. Orlandi, L. Portales, S. Ronchi, M.Ö. Sahin, A. Savoy-Navarro[20], P. Simkina, M. Titov, M. Tornago

Laboratoire Leprince-Ringuet, CNRS/IN2P3, Ecole Polytechnique, Institut Polytechnique de Paris, Palaiseau, France
F. Beaudette, G. Boldrini, P. Busson, C. Charlot, M. Chiusi, T.D. Cuisset, F. Damas, O. Davignon, A. De Wit, T. Debnath, I.T. Ehle, B.A. Fontana Santos Alves, S. Ghosh, A. Gilbert, R. Granier de Cassagnac, L. Kalipoliti, M. Manoni, M. Nguyen, S. Obraztsov, C. Ochando, R. Salerno, J.B. Sauvan, Y. Sirois, G. Sokmen, L. Urda Gómez, A. Zabi, A. Zghiche

Université de Strasbourg, CNRS, IPHC UMR 7178, Strasbourg, France
J.-L. Agram[21], J. Andrea, D. Bloch, J.-M. Brom, E.C. Chabert, C. Collard, G. Coulon, S. Falke, U. Goerlach, R. Haeberle, A.-C. Le Bihan, M. Meena, O. Poncet, G. Saha, P. Vaucelle

Centre de Calcul de l'Institut National de Physique Nucleaire et de Physique des Particules, CNRS/IN2P3, Villeurbanne, France
A. Di Florio

Institut de Physique des 2 Infinis de Lyon (IP2I), Villeurbanne, France
D. Amram, S. Beauceron, B. Blancon, G. Boudoul, N. Chanon, D. Contardo, P. Depasse, C. Dozen[22], H. El Mamouni, J. Fay, S. Gascon, M. Gouzevitch, C. Greenberg, G. Grenier, B. Ille, E. Jourd'huy, I.B. Laktineh, M. Lethuillier, B. Massoteau, L. Mirabito, A. Purohit, M. Vander Donckt, J. Xiao

Georgian Technical University, Tbilisi, Georgia
A. Khvedelidze[23], I. Lomidze, Z. Tsamalaidze[23]

JHEP12(2025)178

RWTH Aachen University, I. Physikalisches Institut, Aachen, Germany
V. Botta, S. Consuegra Rodríguez, L. Feld, K. Klein, M. Lipinski, D. Meuser, P. Nattland, V. Oppenländer, A. Pauls, D. Pérez Adán, N. Röwert, M. Teroerde

RWTH Aachen University, III. Physikalisches Institut A, Aachen, Germany
C. Daumann, S. Diekmann, A. Dodonova, N. Eich, D. Eliseev, F. Engelke, J. Erdmann, M. Erdmann, B. Fischer, T. Hebbeker, K. Hoepfner, F. Ivone, A. Jung, N. Kumar, M.y. Lee, F. Mausolf, M. Merschmeyer, A. Meyer, F. Nowotny, A. Pozdnyakov, W. Redjeb, H. Reithler, U. Sarkar, V. Sarkisovi, A. Schmidt, C. Seth, A. Sharma, J.L. Spah, V. Vaulin, S. Zaleski

RWTH Aachen University, III. Physikalisches Institut B, Aachen, Germany
M.R. Beckers, C. Dziwok, G. Flügge, N. Hoeflich, T. Kress, A. Nowack, O. Pooth, A. Stahl, A. Zotz

Deutsches Elektronen-Synchrotron, Hamburg, Germany
H. Aarup Petersen, A. Abel, M. Aldaya Martin, J. Alimena, S. Amoroso, Y. An, I. Andreev, J. Bach, S. Baxter, M. Bayatmakou, H. Becerril Gonzalez, O. Behnke, A. Belvedere, F. Blekman[24], K. Borras[25], A. Campbell, S. Chatterjee, L.X. Coll Saravia, G. Eckerlin, D. Eckstein, E. Gallo[24], A. Geiser, V. Guglielmi, M. Guthoff, A. Hinzmann, L. Jeppe, M. Kasemann, C. Kleinwort, R. Kogler, M. Komm, D. Krücker, W. Lange, D. Leyva Pernia, K.-Y. Lin, K. Lipka[26], W. Lohmann[27], J. Malvaso, R. Mankel, I.-A. Melzer-Pellmann, M. Mendizabal Morentin, A.B. Meyer, G. Milella, K. Moral Figueroa, A. Mussgiller, L.P. Nair, J. Niedziela, A. Nürnberg, J. Park, E. Ranken, A. Raspereza, D. Rastorguev, L. Rygaard, M. Scham[28,25], S. Schnake[25], P. Schütze, C. Schwanenberger[24], D. Selivanova, K. Sharko, M. Shchedrolosiev, D. Stafford, M. Torkian, F. Vazzoler, A. Ventura Barroso, R. Walsh, D. Wang, Q. Wang, K. Wichmann, L. Wiens[25], C. Wissing, Y. Yang, S. Zakharov, A. Zimermmane Castro Santos

University of Hamburg, Hamburg, Germany
A. Albrecht, A.R. Alves Andrade, M. Antonello, S. Bollweg, M. Bonanomi, K. El Morabit, Y. Fischer, M. Frahm, E. Garutti, A. Grohsjean, A.A. Guvenli, J. Haller, D. Hundhausen, G. Kasieczka, P. Keicher, R. Klanner, W. Korcari, T. Kramer, C.c. Kuo, F. Labe, J. Lange, A. Lobanov, L. Moureaux, M. Mrowietz, A. Nigamova, K. Nikolopoulos, Y. Nissan, A. Paasch, K.J. Pena Rodriguez, N. Prouvost, T. Quadfasel, B. Raciti, M. Rieger, D. Savoiu, P. Schleper, M. Schröder, J. Schwandt, M. Sommerhalder, H. Stadie, G. Steinbrück, A. Tews, R. Ward, B. Wiederspan, M. Wolf

Karlsruher Institut fuer Technologie, Karlsruhe, Germany
S. Brommer, E. Butz, Y.M. Chen, T. Chwalek, A. Dierlamm, G.G. Dincer, U. Elicabuk, N. Faltermann, M. Giffels, A. Gottmann, F. Hartmann[29], R. Hofsaess, M. Horzela, U. Husemann, J. Kieseler, M. Klute, R. Kunnilan Muhammed Rafeek, O. Lavoryk, J.M. Lawhorn, A. Lintuluoto, S. Maier, M. Mormile, Th. Müller, E. Pfeffer, M. Presilla, G. Quast, K. Rabbertz, B. Regnery, R. Schmieder, N. Shadskiy,

JHEP12(2025)178

I. Shvetsov, H.J. Simonis, L. Sowa, L. Stockmeier, K. Tauqeer, M. Toms, B. Topko, N. Trevisani, C. Verstege, T. Voigtländer, R.F. Von Cube, J. Von Den Driesch, M. Wassmer, R. Wolf, W.D. Zeuner, X. Zuo

Institute of Nuclear and Particle Physics (INPP), NCSR Demokritos, Aghia Paraskevi, Greece

G. Anagnostou, G. Daskalakis, A. Kyriakis

National and Kapodistrian University of Athens, Athens, Greece

G. Melachroinos, Z. Painesis, I. Paraskevas, N. Saoulidou, K. Theofilatos, E. Tziaferi, E. Tzovara, K. Vellidis, I. Zisopoulos

National Technical University of Athens, Athens, Greece

T. Chatzistavrou, G. Karapostoli, K. Kousouris, E. Siamarkou, G. Tsipolitis

University of Ioánnina, Ioánnina, Greece

I. Bestintzanos, I. Evangelou, C. Foudas, P. Katsoulis, P. Kokkas, P.G. Kosmoglou Kioseoglou, N. Manthos, I. Papadopoulos, J. Strologas

HUN-REN Wigner Research Centre for Physics, Budapest, Hungary

D. Druzhkin, C. Hajdu, D. Horvath[30,31], K. Márton, A.J. Rádl[32], F. Sikler, V. Veszpremi

MTA-ELTE Lendület CMS Particle and Nuclear Physics Group, Eötvös Loránd University, Budapest, Hungary

M. Csanád, K. Farkas, A. Fehérkuti[33], M.M.A. Gadallah[34], Á. Kadlecsik, M. León Coello, G. Pásztor, G.I. Veres

Faculty of Informatics, University of Debrecen, Debrecen, Hungary

B. Ujvari, G. Zilizi

HUN-REN ATOMKI — Institute of Nuclear Research, Debrecen, Hungary

G. Bencze, S. Czellar, J. Molnar, Z. Szillasi

Karoly Robert Campus, MATE Institute of Technology, Gyongyos, Hungary

T. Csorgo[33], F. Nemes[33], T. Novak, I. Szanyi[35]

Panjab University, Chandigarh, India

S. Bansal, S.B. Beri, V. Bhatnagar, G. Chaudhary, S. Chauhan, N. Dhingra[36], A. Kaur, A. Kaur, H. Kaur, M. Kaur, S. Kumar, T. Sheokand, J.B. Singh, A. Singla

University of Delhi, Delhi, India

A. Bhardwaj, A. Chhetri, B.C. Choudhary, A. Kumar, A. Kumar, M. Naimuddin, S. Phor, K. Ranjan, M.K. Saini

University of Hyderabad, Hyderabad, India

S. Acharya[37], B. Gomber[37], B. Sahu[37]

JHEP12(2025)178

Indian Institute of Technology Kanpur, Kanpur, India
S. Mukherjee

Saha Institute of Nuclear Physics, HBNI, Kolkata, India
S. Baradia, S. Bhattacharya, S. Das Gupta, S. Dutta, S. Dutta, S. Sarkar

Indian Institute of Technology Madras, Madras, India
M.M. Ameen, P.K. Behera, S. Chatterjee, G. Dash, A. Dattamunsi, P. Jana, P. Kalbhor, S. Kamble, J.R. Komaragiri[38], T. Mishra, P.R. Pujahari, A.K. Sikdar, R.K. Singh, P. Verma, S. Verma, A. Vijay

IISER Mohali, India, Mohali, India
B.K. Sirasva

Tata Institute of Fundamental Research-A, Mumbai, India
L. Bhatt, S. Dugad, G.B. Mohanty, M. Shelake, P. Suryadevara

Tata Institute of Fundamental Research-B, Mumbai, India
A. Bala, S. Banerjee, S. Barman[39], R.M. Chatterjee, M. Guchait, Sh. Jain, A. Jaiswal, B.M. Joshi, S. Kumar, M. Maity[39], G. Majumder, K. Mazumdar, S. Parolia, R. Saxena, A. Thachayath

National Institute of Science Education and Research, An OCC of Homi Bhabha National Institute, Bhubaneswar, Odisha, India
S. Bahinipati[40], D. Maity[41], P. Mal, K. Naskar[41], A. Nayak[41], S. Nayak, K. Pal, R. Raturi, P. Sadangi, S.K. Swain, S. Varghese[41], D. Vats[41]

Indian Institute of Science Education and Research (IISER), Pune, India
A. Alpana, S. Dube, P. Hazarika, B. Kansal, A. Laha, R. Sharma, S. Sharma, K.Y. Vaish

Indian Institute of Technology Hyderabad, Telangana, India
S. Ghosh

Isfahan University of Technology, Isfahan, Iran
H. Bakhshiansohi[42], A. Jafari[43], V. Sedighzadeh Dalavi, M. Zeinali[44]

Institute for Research in Fundamental Sciences (IPM), Tehran, Iran
S. Bashiri, S. Chenarani[45], S.M. Etesami, Y. Hosseini, M. Khakzad, E. Khazaie, M. Mohammadi Najafabadi, S. Tizchang[46]

University College Dublin, Dublin, Ireland
M. Felcini, M. Grunewald

INFN Sezione di Bari[a], Università di Bari[b], Politecnico di Bari[c], Bari, Italy
M. Abbrescia[a,b], M. Barbieri[a,b], M. Buonsante[a,b], A. Colaleo[a,b], D. Creanza[a,c], B. D'Anzi[a,b], N. De Filippis[a,c], M. De Palma[a,b], W. Elmetenawee[a,b,47], N. Ferrara[a,c],

JHEP12(2025)178

L. Fiore[a], L. Longo[a], M. Louka[a,b], G. Maggi[a,c], M. Maggi[a], I. Margjeka[a], V. Mastrapasqua[a,b], S. My[a,b], F. Nenna[a,b], S. Nuzzo[a,b], A. Pellecchia[a,b], A. Pompili[a,b], G. Pugliese[a,c], R. Radogna[a,b], D. Ramos[a], A. Ranieri[a], L. Silvestris[a], F.M. Simone[a,c], Ü. Sözbilir[a], A. Stamerra[a,b], D. Troiano[a,b], R. Venditti[a,b], P. Verwilligen[a], A. Zaza[a,b]

INFN Sezione di Bologna[a], Università di Bologna[b], Bologna, Italy

G. Abbiendi[a], C. Battilana[a,b], D. Bonacorsi[a,b], P. Capiluppi[a,b], F.R. Cavallo[a], M. Cuffiani[a,b], G.M. Dallavalle[a], T. Diotalevi[a,b], F. Fabbri[a], A. Fanfani[a,b], D. Fasanella[a], P. Giacomelli[a], C. Grandi[a], L. Guiducci[a,b], S. Lo Meo[a,48], M. Lorusso[a,b], L. Lunerti[a], G. Masetti[a], F.L. Navarria[a,b], G. Paggi[a,b], A. Perrotta[a], F. Primavera[a,b], A.M. Rossi[a,b], S. Rossi Tisbeni[a,b], T. Rovelli[a,b], G.P. Siroli[a,b]

INFN Sezione di Catania[a], Università di Catania[b], Catania, Italy

S. Costa[a,b,49], A. Di Mattia[a], A. Lapertosa[a], R. Potenza[a,b], A. Tricomi[a,b,49]

INFN Sezione di Firenze[a], Università di Firenze[b], Firenze, Italy

J. Altork[a,b], P. Assiouras[a], G. Barbagli[a], G. Bardelli[a], M. Bartolini[a,b], A. Calandri[a,b], B. Camaiani[a,b], A. Cassese[a], R. Ceccarelli[a], V. Ciulli[a,b], C. Civinini[a], R. D'Alessandro[a,b], L. Damenti[a,b], E. Focardi[a,b], T. Kello[a], G. Latino[a,b], P. Lenzi[a,b], M. Lizzo[a], M. Meschini[a], S. Paoletti[a], A. Papanastassiou[a,b], G. Sguazzoni[a], L. Viliani[a]

INFN Laboratori Nazionali di Frascati, Frascati, Italy

L. Benussi, S. Colafranceschi[50], S. Meola[51], D. Piccolo

INFN Sezione di Genova[a], Università di Genova[b], Genova, Italy

M. Alves Gallo Pereira[a], F. Ferro[a], E. Robutti[a], S. Tosi[a,b]

INFN Sezione di Milano-Bicocca[a], Università di Milano-Bicocca[b], Milano, Italy

A. Benaglia[a], F. Brivio[a], V. Camagni[a,b], F. Cetorelli[a,b], F. De Guio[a,b], M.E. Dinardo[a,b], P. Dini[a], S. Gennai[a], R. Gerosa[a,b], A. Ghezzi[a,b], P. Govoni[a,b], L. Guzzi[a], M.R. Kim[a], G. Lavizzari[a,b], M.T. Lucchini[a,b], M. Malberti[a], S. Malvezzi[a], A. Massironi[a], D. Menasce[a], L. Moroni[a], M. Paganoni[a,b], S. Palluotto[a,b], D. Pedrini[a], A. Perego[a,b], B.S. Pinolini[a], G. Pizzati[a,b], S. Ragazzi[a,b], T. Tabarelli de Fatis[a,b]

INFN Sezione di Napoli[a], Università di Napoli 'Federico II'[b], Napoli, Italy; Università della Basilicata[c], Potenza, Italy; Scuola Superiore Meridionale (SSM)[d], Napoli, Italy

S. Buontempo[a], C. Di Fraia[a,b], F. Fabozzi[a,c], L. Favilla[a,d], A.O.M. Iorio[a,b], L. Lista[a,b,52], P. Paolucci[a,29], B. Rossi[a]

INFN Sezione di Padova[a], Università di Padova[b], Padova, Italy; Universita degli Studi di Cagliari[c], Cagliari, Italy

P. Azzi[a], N. Bacchetta[a,53], D. Bisello[a,b], P. Bortignon[a,c], G. Bortolato[a,b], A.C.M. Bulla[a,c], R. Carlin[a,b], T. Dorigo[a,54], U. Gasparini[a,b], S. Giorgetti[a], E. Lusiani[a], M. Margoni[a,b], A.T. Meneguzzo[a,b], M. Passaseo[a], J. Pazzini[a,b], P. Ronchese[a,b], R. Rossin[a,b],

JHEP12(2025)178

F. Simonetto[a,b], M. Tosi[a,b], A. Triossi[a,b], S. Ventura[a], M. Zanetti[a,b], P. Zotto[a,b], A. Zucchetta[a,b], G. Zumerle[a,b]

INFN Sezione di Pavia[a], Università di Pavia[b], Pavia, Italy

A. Braghieri[a], S. Calzaferri[a], P. Montagna[a,b], M. Pelliccioni[a], V. Re[a], C. Riccardi[a,b], P. Salvini[a], I. Vai[a,b], P. Vitulo[a,b]

INFN Sezione di Perugia[a], Università di Perugia[b], Perugia, Italy

S. Ajmal[a,b], M.E. Ascioti[a,b], G.M. Bilei[a], C. Carrivale[a,b], D. Ciangottini[a,b], L. Della Penna[a,b], L. Fanò[a,b], V. Mariani[a,b], M. Menichelli[a], F. Moscatelli[a,55], A. Rossi[a,b], A. Santocchia[a,b], D. Spiga[a], T. Tedeschi[a,b]

INFN Sezione di Pisa[a], Università di Pisa[b], Scuola Normale Superiore di Pisa[c], Pisa, Italy; Università di Siena[d], Siena, Italy

C. Aimè[a,b], C.A. Alexe[a,c], P. Asenov[a,b], P. Azzurri[a], G. Bagliesi[a], R. Bhattacharya[a], L. Bianchini[a,b], T. Boccali[a], E. Bossini[a], D. Bruschini[a,c], L. Calligaris[a,b], R. Castaldi[a], F. Cattafesta[a,c], M.A. Ciocci[a,d], M. Cipriani[a,b], R. Dell'Orso[a], S. Donato[a,b], R. Forti[a,b], A. Giassi[a], F. Ligabue[a,c], A.C. Marini[a,b], D. Matos Figueiredo[a], A. Messineo[a,b], S. Mishra[a], V.K. Muraleedharan Nair Bindhu[a,b], S. Nandan[a], F. Palla[a], M. Riggirello[a,c], A. Rizzi[a,b], G. Rolandi[a,c], S. Roy Chowdhury[a,56], T. Sarkar[a], A. Scribano[a], P. Solanki[a,b], P. Spagnolo[a], F. Tenchini[a,b], R. Tenchini[a], G. Tonelli[a,b], N. Turini[a,d], F. Vaselli[a,c], A. Venturi[a], P.G. Verdini[a]

INFN Sezione di Roma[a], Sapienza Università di Roma[b], Roma, Italy

P. Akrap[a,b], C. Basile[a,b], S.C. Behera[a], F. Cavallari[a], L. Cunqueiro Mendez[a,b], F. De Riggi[a,b], D. Del Re[a,b], E. Di Marco[a], F. Errico[a], L. Frosina[a,b], R. Gargiulo[a,b], B. Harikrishnan[a,b], F. Lombardi[a,b], E. Longo[a,b], L. Martikainen[a,b], J. Mijuskovic[a,b], G. Organtini[a,b], N. Palmeri[a,b], F. Pandolfi[a], R. Paramatti[a,b], C. Quaranta[a,b], S. Rahatlou[a,b], C. Rovelli[a], F. Santanastasio[a,b], L. Soffi[a], V. Vladimirov[a,b]

INFN Sezione di Torino[a], Università di Torino[b], Torino, Italy; Università del Piemonte Orientale[c], Novara, Italy

N. Amapane[a,b], R. Arcidiacono[a,c], S. Argiro[a,b], M. Arneodo[a,c], N. Bartosik[a,c], R. Bellan[a,b], A. Bellora[a,b], C. Biino[a], C. Borca[a,b], N. Cartiglia[a], M. Costa[a,b], R. Covarelli[a,b], N. Demaria[a], L. Finco[a], M. Grippo[a,b], B. Kiani[a,b], L. Lanteri[a,b], F. Legger[a], F. Luongo[a,b], C. Mariotti[a], S. Maselli[a], A. Mecca[a,b], L. Menzio[a,b], P. Meridiani[a], E. Migliore[a,b], M. Monteno[a], M.M. Obertino[a,b], G. Ortona[a], L. Pacher[a,b], N. Pastrone[a], M. Ruspa[a,c], F. Siviero[a,b], V. Sola[a,b], A. Solano[a,b], A. Staiano[a], C. Tarricone[a,b], D. Trocino[a], G. Umoret[a,b], E. Vlasov[a,b], R. White[a,b]

INFN Sezione di Trieste[a], Università di Trieste[b], Trieste, Italy

J. Babbar[a,b], S. Belforte[a], V. Candelise[a,b], M. Casarsa[a], F. Cossutti[a], K. De Leo[a], G. Della Ricca[a,b], R. Delli Gatti[a,b]

JHEP12(2025)178

Kyungpook National University, Daegu, Korea
S. Dogra, J. Hong, J. Kim, T. Kim, D. Lee, H. Lee, J. Lee, S.W. Lee, C.S. Moon, Y.D. Oh, S. Sekmen, B. Tae, Y.C. Yang

Department of Mathematics and Physics — GWNU, Gangneung, Korea
M.S. Kim

Chonnam National University, Institute for Universe and Elementary Particles, Kwangju, Korea
G. Bak, P. Gwak, H. Kim, D.H. Moon, J. Seo

Hanyang University, Seoul, Korea
E. Asilar, F. Carnevali, J. Choi[57], T.J. Kim, Y. Ryou

Korea University, Seoul, Korea
S. Ha, S. Han, B. Hong, J. Kim, K. Lee, K.S. Lee, S. Lee, J. Yoo

Kyung Hee University, Department of Physics, Seoul, Korea
J. Goh, J. Shin, S. Yang

Sejong University, Seoul, Korea
Y. Kang, H. S. Kim, Y. Kim, S. Lee

Seoul National University, Seoul, Korea
J. Almond, J.H. Bhyun, J. Choi, J. Choi, W. Jun, H. Kim, J. Kim, T. Kim, Y. Kim, Y.W. Kim, S. Ko, H. Lee, J. Lee, J. Lee, B.H. Oh, S.B. Oh, J. Shin, U.K. Yang, I. Yoon

University of Seoul, Seoul, Korea
W. Jang, D.Y. Kang, D. Kim, S. Kim, B. Ko, J.S.H. Lee, Y. Lee, I.C. Park, Y. Roh, I.J. Watson

Yonsei University, Department of Physics, Seoul, Korea
G. Cho, K. Hwang, B. Kim, S. Kim, K. Lee, H.D. Yoo

Sungkyunkwan University, Suwon, Korea
M. Choi, Y. Lee, I. Yu

College of Engineering and Technology, American University of the Middle East (AUM), Dasman, Kuwait
T. Beyrouthy, Y. Gharbia

Kuwait University — College of Science — Department of Physics, Safat, Kuwait
F. Alazemi

Riga Technical University, Riga, Latvia
K. Dreimanis, O.M. Eberlins, A. Gaile, C. Munoz Diaz, D. Osite, G. Pikurs, R. Plese, A. Potrebko, M. Seidel, D. Sidiropoulos Kontos

JHEP12(2025)178

University of Latvia (LU), Riga, Latvia
N.R. Strautnieks

Vilnius University, Vilnius, Lithuania
M. Ambrozas, A. Juodagalvis, S. Nargelas, A. Rinkevicius, G. Tamulaitis

National Centre for Particle Physics, Universiti Malaya, Kuala Lumpur, Malaysia
I. Yusuff[58], Z. Zolkapli

Universidad de Sonora (UNISON), Hermosillo, Mexico
J.F. Benitez, A. Castaneda Hernandez, A. Cota Rodriguez, L.E. Cuevas Picos, H.A. Encinas Acosta, L.G. Gallegos Maríñez, J.A. Murillo Quijada, A. Sehrawat, L. Valencia Palomo

Centro de Investigacion y de Estudios Avanzados del IPN, Mexico City, Mexico
G. Ayala, H. Castilla-Valdez, H. Crotte Ledesma, R. Lopez-Fernandez, J. Mejia Guisao, R. Reyes-Almanza, A. Sánchez Hernández

Universidad Iberoamericana, Mexico City, Mexico
C. Oropeza Barrera, D.L. Ramirez Guadarrama, M. Ramírez García

Benemerita Universidad Autonoma de Puebla, Puebla, Mexico
I. Bautista, F.E. Neri Huerta, I. Pedraza, H.A. Salazar Ibarguen, C. Uribe Estrada

University of Montenegro, Podgorica, Montenegro
I. Bubanja, N. Raicevic

University of Canterbury, Christchurch, New Zealand
P.H. Butler

National Centre for Physics, Quaid-I-Azam University, Islamabad, Pakistan
A. Ahmad, M.I. Asghar, A. Awais, M.I.M. Awan, W.A. Khan

AGH University of Krakow, Krakow, Poland
V. Avati, L. Forthomme, L. Grzanka, M. Malawski, K. Piotrzkowski

National Centre for Nuclear Research, Swierk, Poland
M. Bluj, M. Górski, M. Kazana, M. Szleper, P. Zalewski

Institute of Experimental Physics, Faculty of Physics, University of Warsaw, Warsaw, Poland
K. Bunkowski, K. Doroba, A. Kalinowski, M. Konecki, J. Krolikowski, A. Muhammad

Warsaw University of Technology, Warsaw, Poland
P. Fokow, K. Pozniak, W. Zabolotny

JHEP12(2025)178

Laboratório de Instrumentação e Física Experimental de Partículas, Lisboa, Portugal

M. Araujo, D. Bastos, C. Beirão Da Cruz E Silva, A. Boletti, M. Bozzo, T. Camporesi, G. Da Molin, M. Gallinaro, J. Hollar, N. Leonardo, G.B. Marozzo, A. Petrilli, M. Pisano, J. Seixas, J. Varela, J.W. Wulff

Faculty of Physics, University of Belgrade, Belgrade, Serbia

P. Adzic, L. Markovic, P. Milenovic, V. Milosevic

VINCA Institute of Nuclear Sciences, University of Belgrade, Belgrade, Serbia

D. Devetak, M. Dordevic, J. Milosevic, L. Nadderd, V. Rekovic, M. Stojanovic

Centro de Investigaciones Energéticas Medioambientales y Tecnológicas (CIEMAT), Madrid, Spain

M. Alcalde Martinez, J. Alcaraz Maestre, Cristina F. Bedoya, J.A. Brochero Cifuentes, Oliver M. Carretero, M. Cepeda, M. Cerrada, N. Colino, J. Cuchillo Ortega, B. De La Cruz, A. Delgado Peris, A. Escalante Del Valle, D. Fernández Del Val, J.P. Fernández Ramos, J. Flix, M.C. Fouz, M. Gonzalez Hernandez, O. Gonzalez Lopez, S. Goy Lopez, J.M. Hernandez, M.I. Josa, J. Llorente Merino, C. Martin Perez, E. Martin Viscasillas, D. Moran, C. M. Morcillo Perez, R. Paz Herrera, C. Perez Dengra, A. Pérez-Calero Yzquierdo, J. Puerta Pelayo, I. Redondo, J. Vazquez Escobar

Universidad Autónoma de Madrid, Madrid, Spain

J.F. de Trocóniz

Universidad de Oviedo, Instituto Universitario de Ciencias y Tecnologías Espaciales de Asturias (ICTEA), Oviedo, Spain

B. Alvarez Gonzalez, J. Ayllon Torresano, A. Cardini, J. Cuevas, J. Del Riego Badas, D. Estrada Acevedo, J. Fernandez Menendez, S. Folgueras, I. Gonzalez Caballero, P. Leguina, M. Obeso Menendez, E. Palencia Cortezon, J. Prado Pico, A. Soto Rodríguez, C. Vico Villalba, P. Vischia

Instituto de Física de Cantabria (IFCA), CSIC-Universidad de Cantabria, Santander, Spain

S. Blanco Fernández, I.J. Cabrillo, A. Calderon, J. Duarte Campderros, M. Fernandez, G. Gomez, C. Lasaosa García, R. Lopez Ruiz, C. Martinez Rivero, P. Martinez Ruiz del Arbol, F. Matorras, P. Matorras Cuevas, E. Navarrete Ramos, J. Piedra Gomez, C. Quintana San Emeterio, L. Scodellaro, I. Vila, R. Vilar Cortabitarte, J.M. Vizan Garcia

University of Colombo, Colombo, Sri Lanka

B. Kailasapathy[59], D.D.C. Wickramarathna

University of Ruhuna, Department of Physics, Matara, Sri Lanka

W.G.D. Dharmaratna[60], K. Liyanage, N. Perera

JHEP12(2025)178

CERN, European Organization for Nuclear Research, Geneva, Switzerland
D. Abbaneo, C. Amendola, R. Ardino, E. Auffray, J. Baechler, D. Barney, M. Bianco, A. Bocci, L. Borgonovi, C. Botta, A. Bragagnolo, C.E. Brown, C. Caillol, G. Cerminara, P. Connor, D. d'Enterria, A. Dabrowski, A. David, A. De Roeck, M.M. Defranchis, M. Deile, M. Dobson, W. Funk, A. Gaddi, S. Giani, D. Gigi, K. Gill, F. Glege, M. Glowacki, A. Gruber, J. Hegeman, J.K. Heikkilä, B. Huber, V. Innocente, T. James, P. Janot, O. Kaluzinska, O. Karacheban[27], G. Karathanasis, S. Laurila, P. Lecoq, C. Lourenço, A.-M. Lyon, M. Magherini, L. Malgeri, M. Mannelli, A. Mehta, F. Meijers, J.A. Merlin, S. Mersi, E. Meschi, M. Migliorini, F. Monti, F. Moortgat, M. Mulders, M. Musich, I. Neutelings, S. Orfanelli, F. Pantaleo, M. Pari, G. Petrucciani, A. Pfeiffer, M. Pierini, M. Pitt, H. Qu, D. Rabady, B. Ribeiro Lopes, F. Riti, P. Rosado, M. Rovere, H. Sakulin, R. Salvatico, S. Sanchez Cruz, S. Scarfi, M. Selvaggi, A. Sharma, K. Shchelina, P. Silva, P. Sphicas[61], A.G. Stahl Leiton, A. Steen, S. Summers, D. Treille, P. Tropea, E. Vernazza, J. Wanczyk[62], J. Wang, S. Wuchterl, M. Zarucki, P. Zehetner, P. Zejdl, G. Zevi Della Porta

PSI Center for Neutron and Muon Sciences, Villigen, Switzerland
T. Bevilacqua[63], L. Caminada[63], W. Erdmann, R. Horisberger, Q. Ingram, H.C. Kaestli, D. Kotlinski, C. Lange, U. Langenegger, M. Missiroli[63], L. Noehte[63], T. Rohe, A. Samalan

ETH Zurich — Institute for Particle Physics and Astrophysics (IPA), Zurich, Switzerland
T.K. Aarrestad, M. Backhaus, G. Bonomelli, C. Cazzaniga, K. Datta, P. De Bryas Dexmiers D'archiacchiac[62], A. De Cosa, G. Dissertori, M. Dittmar, M. Donegà, F. Eble, K. Gedia, F. Glessgen, C. Grab, N. Härringer, T.G. Harte, W. Lustermann, M. Malucchi, R.A. Manzoni, M. Marchegiani, L. Marchese, A. Mascellani[62], F. Nessi-Tedaldi, F. Pauss, V. Perovic, B. Ristic, R. Seidita, J. Steggemann[62], A. Tarabini, D. Valsecchi, R. Wallny

Universität Zürich, Zurich, Switzerland
C. Amsler[64], P. Bärtschi, F. Bilandzija, M.F. Canelli, G. Celotto, K. Cormier, M. Huwiler, W. Jin, A. Jofrehei, B. Kilminster, T.H. Kwok, S. Leontsinis, V. Lukashenko, A. Macchiolo, F. Meng, J. Motta, A. Reimers, P. Robmann, M. Senger, E. Shokr, F. Stäger, R. Tramontano

National Central University, Chung-Li, Taiwan
D. Bhowmik, C.M. Kuo, P.K. Rout, S. Taj, P.C. Tiwari[38]

National Taiwan University (NTU), Taipei, Taiwan
L. Ceard, K.F. Chen, Z.g. Chen, A. De Iorio, W.-S. Hou, T.h. Hsu, Y.w. Kao, S. Karmakar, G. Kole, Y.y. Li, R.-S. Lu, E. Paganis, X.f. Su, J. Thomas-Wilsker, L.s. Tsai, D. Tsionou, H.y. Wu, E. Yazgan

JHEP12(2025)178

High Energy Physics Research Unit, Department of Physics, Faculty of Science, Chulalongkorn University, Bangkok, Thailand

C. Asawatangtrakuldee, N. Srimanobhas

Tunis El Manar University, Tunis, Tunisia

Y. Maghrbi

Çukurova University, Physics Department, Science and Art Faculty, Adana, Turkey

D. Agyel, F. Dolek, I. Dumanoglu[65], Y. Guler[66], E. Gurpinar Guler[66], C. Isik, O. Kara, A. Kayis Topaksu, Y. Komurcu, G. Onengut, K. Ozdemir[67], B. Tali[68], U.G. Tok, E. Uslan, I.S. Zorbakir

Middle East Technical University, Physics Department, Ankara, Turkey

M. Yalvac[69]

Bogazici University, Istanbul, Turkey

B. Akgun, I.O. Atakisi[70], E. Gülmez, M. Kaya[71], O. Kaya[72], M.A. Sarkisla[73], S. Tekten[74]

Istanbul Technical University, Istanbul, Turkey

A. Cakir, K. Cankocak[65,75], S. Sen[76]

Istanbul University, Istanbul, Turkey

O. Aydilek[77], B. Hacisahinoglu, I. Hos[78], B. Kaynak, S. Ozkorucuklu, O. Potok, H. Sert, C. Simsek, C. Zorbilmez

Yildiz Technical University, Istanbul, Turkey

S. Cerci, B. Isildak[79], E. Simsek, D. Sunar Cerci, T. Yetkin[22]

Institute for Scintillation Materials of National Academy of Science of Ukraine, Kharkiv, Ukraine

A. Boyaryntsev, O. Dadazhanova, B. Grynyov

National Science Centre, Kharkiv Institute of Physics and Technology, Kharkiv, Ukraine

L. Levchuk

University of Bristol, Bristol, United Kingdom

J.J. Brooke, A. Bundock, F. Bury, E. Clement, D. Cussans, D. Dharmender, H. Flacher, J. Goldstein, H.F. Heath, M.-L. Holmberg, L. Kreczko, S. Paramesvaran, L. Robertshaw, M.S. Sanjrani[42], J. Segal, V.J. Smith

Rutherford Appleton Laboratory, Didcot, United Kingdom

A.H. Ball, K.W. Bell, A. Belyaev[80], C. Brew, R.M. Brown, D.J.A. Cockerill, A. Elliot, K.V. Ellis, J. Gajownik, K. Harder, S. Harper, J. Linacre, K. Manolopoulos, M. Moallemi,

JHEP12(2025)178

D.M. Newbold, E. Olaiya, D. Petyt, T. Reis, A.R. Sahasransu, G. Salvi, T. Schuh, C.H. Shepherd-Themistocleous, I.R. Tomalin, K.C. Whalen, T. Williams

Imperial College, London, United Kingdom

I. Andreou, R. Bainbridge, P. Bloch, O. Buchmuller, C.A. Carrillo Montoya, D. Colling, J.S. Dancu, I. Das, P. Dauncey, G. Davies, M. Della Negra, S. Fayer, G. Fedi, G. Hall, H.R. Hoorani, A. Howard, G. Iles, C.R. Knight, P. Krueper, J. Langford, K.H. Law, J. León Holgado, E. Leutgeb, L. Lyons, A.-M. Magnan, B. Maier, S. Mallios, A. Mastronikolis, M. Mieskolainen, J. Nash[81], M. Pesaresi, P.B. Pradeep, B.C. Radburn-Smith, A. Richards, A. Rose, L. Russell, K. Savva, C. Seez, R. Shukla, A. Tapper, K. Uchida, G.P. Uttley, T. Virdee[29], M. Vojinovic, N. Wardle, D. Winterbottom

Brunel University, Uxbridge, United Kingdom

J.E. Cole, A. Khan, P. Kyberd, I.D. Reid

Baylor University, Waco, Texas, U.S.A.

S. Abdullin, A. Brinkerhoff, E. Collins, M.R. Darwish, J. Dittmann, K. Hatakeyama, V. Hegde, J. Hiltbrand, B. McMaster, J. Samudio, S. Sawant, C. Sutantawibul, J. Wilson

Bethel University, St. Paul, Minnesota, U.S.A.

J.M. Hogan[82]

Catholic University of America, Washington, DC, U.S.A.

R. Bartek, A. Dominguez, S. Raj, A.E. Simsek, S.S. Yu

The University of Alabama, Tuscaloosa, Alabama, U.S.A.

B. Bam, A. Buchot Perraguin, S. Campbell, R. Chudasama, S.I. Cooper, C. Crovella, G. Fidalgo, S.V. Gleyzer, A. Khukhunaishvili, K. Matchev, E. Pearson, C.U. Perez, P. Rumerio[83], E. Usai, R. Yi

Boston University, Boston, Massachusetts, U.S.A.

S. Cholak, G. De Castro, Z. Demiragli, C. Erice, C. Fangmeier, C. Fernandez Madrazo, E. Fontanesi, J. Fulcher, F. Golf, S. Jeon, J. O'Cain, I. Reed, J. Rohlf, K. Salyer, D. Sperka, D. Spitzbart, I. Suarez, A. Tsatsos, E. Wurtz, A.G. Zecchinelli

Brown University, Providence, Rhode Island, U.S.A.

G. Barone, G. Benelli, D. Cutts, S. Ellis, L. Gouskos, M. Hadley, U. Heintz, K.W. Ho, T. Kwon, G. Landsberg, K.T. Lau, J. Luo, S. Mondal, J. Roloff, T. Russell, S. Sagir[84], X. Shen, M. Stamenkovic, N. Venkatasubramanian

University of California, Davis, Davis, California, U.S.A.

S. Abbott, B. Barton, R. Breedon, H. Cai, M. Calderon De La Barca Sanchez, M. Chertok, M. Citron, J. Conway, P.T. Cox, R. Erbacher, O. Kukral, G. Mocellin, S. Ostrom, I. Salazar Segovia, W. Wei, S. Yoo

University of California, Los Angeles, California, U.S.A.
K. Adamidis, M. Bachtis, D. Campos, R. Cousins, A. Datta, G. Flores Avila, J. Hauser, M. Ignatenko, M.A. Iqbal, T. Lam, Y.f. Lo, E. Manca, A. Nunez Del Prado, D. Saltzberg, V. Valuev

University of California, Riverside, Riverside, California, U.S.A.
R. Clare, J.W. Gary, G. Hanson

University of California, San Diego, La Jolla, California, U.S.A.
A. Aportela, A. Arora, J.G. Branson, S. Cittolin, S. Cooperstein, D. Diaz, J. Duarte, L. Giannini, Y. Gu, J. Guiang, V. Krutelyov, R. Lee, J. Letts, H. Li, M. Masciovecchio, F. Mokhtar, S. Mukherjee, M. Pieri, D. Primosch, M. Quinnan, V. Sharma, M. Tadel, E. Vourliotis, F. Würthwein, A. Yagil, Z. Zhao

University of California, Santa Barbara — Department of Physics, Santa Barbara, California, U.S.A.
A. Barzdukas, L. Brennan, C. Campagnari, S. Carron Montero[85], K. Downham, C. Grieco, M.M. Hussain, J. Incandela, M.W.K. Lai, A.J. Li, P. Masterson, J. Richman, S.N. Santpur, U. Sarica, R. Schmitz, F. Setti, J. Sheplock, D. Stuart, T.Á. Vámi, X. Yan, D. Zhang

California Institute of Technology, Pasadena, California, U.S.A.
A. Albert, S. Bhattacharya, A. Bornheim, O. Cerri, R. Kansal, J. Mao, H.B. Newman, G. Reales Gutiérrez, T. Sievert, M. Spiropulu, J.R. Vlimant, R.A. Wynne, S. Xie

Carnegie Mellon University, Pittsburgh, Pennsylvania, U.S.A.
J. Alison, S. An, M. Cremonesi, V. Dutta, E.Y. Ertorer, T. Ferguson, T.A. Gómez Espinosa, A. Harilal, A. Kallil Tharayil, M. Kanemura, C. Liu, P. Meiring, T. Mudholkar, S. Murthy, P. Palit, K. Park, M. Paulini, A. Roberts, A. Sanchez, W. Terrill

University of Colorado Boulder, Boulder, Colorado, U.S.A.
J.P. Cumalat, W.T. Ford, A. Hart, A. Hassani, S. Kwan, J. Pearkes, C. Savard, N. Schonbeck, K. Stenson, K.A. Ulmer, S.R. Wagner, N. Zipper, D. Zuolo

Cornell University, Ithaca, New York, U.S.A.
J. Alexander, X. Chen, D.J. Cranshaw, J. Dickinson, J. Fan, X. Fan, J. Grassi, S. Hogan, P. Kotamnives, J. Monroy, G. Niendorf, M. Oshiro, J.R. Patterson, M. Reid, A. Ryd, J. Thom, P. Wittich, R. Zou, L. Zygala

Fermi National Accelerator Laboratory, Batavia, Illinois, U.S.A.
M. Albrow, M. Alyari, O. Amram, G. Apollinari, A. Apresyan, L.A.T. Bauerdick, D. Berry, J. Berryhill, P.C. Bhat, K. Burkett, J.N. Butler, A. Canepa, G.B. Cerati, H.W.K. Cheung, F. Chlebana, C. Cosby, G. Cummings, I. Dutta, V.D. Elvira, J. Freeman, A. Gandrakota, Z. Gecse, L. Gray, D. Green, A. Grummer, S. Grünendahl, D. Guerrero, O. Gutsche, R.M. Harris, T.C. Herwig, J. Hirschauer, B. Jayatilaka,

JHEP12(2025)178

S. Jindariani, M. Johnson, U. Joshi, T. Klijnsma, B. Klima, K.H.M. Kwok, S. Lammel, C. Lee, D. Lincoln, R. Lipton, T. Liu, K. Maeshima, D. Mason, P. McBride, P. Merkel, S. Mrenna, S. Nahn, J. Ngadiuba, D. Noonan, S. Norberg, V. Papadimitriou, N. Pastika, K. Pedro, C. Pena[86], C.E. Perez Lara, F. Ravera, A. Reinsvold Hall[87], L. Ristori, M. Safdari, E. Sexton-Kennedy, N. Smith, A. Soha, L. Spiegel, S. Stoynev, J. Strait, L. Taylor, S. Tkaczyk, N.V. Tran, L. Uplegger, E.W. Vaandering, C. Wang, I. Zoi

University of Florida, Gainesville, Florida, U.S.A.

C. Aruta, P. Avery, D. Bourilkov, P. Chang, V. Cherepanov, R.D. Field, C. Huh, E. Koenig, M. Kolosova, J. Konigsberg, A. Korytov, N. Menendez, G. Mitselmakher, K. Mohrman, A. Muthirakalayil Madhu, N. Rawal, S. Rosenzweig, V. Sulimov, Y. Takahashi, J. Wang

Florida State University, Tallahassee, Florida, U.S.A.

T. Adams, A. Al Kadhim, A. Askew, S. Bower, R. Hashmi, R.S. Kim, T. Kolberg, G. Martinez, M. Mazza, H. Prosper, P.R. Prova, M. Wulansatiti, R. Yohay

Florida Institute of Technology, Melbourne, Florida, U.S.A.

B. Alsufyani, S. Butalla, S. Das, M. Hohlmann, M. Lavinsky, E. Yanes

University of Illinois Chicago, Chicago, Illinois, U.S.A.

M.R. Adams, N. Barnett, A. Baty, C. Bennett, R. Cavanaugh, R. Escobar Franco, O. Evdokimov, C.E. Gerber, H. Gupta, M. Hawksworth, A. Hingrajiya, D.J. Hofman, J.h. Lee, D. S. Lemos, C. Mills, S. Nanda, G. Nigmatkulov, B. Ozek, T. Phan, D. Pilipovic, R. Pradhan, E. Prifti, P. Roy, T. Roy, N. Singh, M.B. Tonjes, N. Varelas, M.A. Wadud, J. Yoo

The University of Iowa, Iowa City, Iowa, U.S.A.

M. Alhusseini, D. Blend, K. Dilsiz[88], O.K. Köseyan, A. Mestvirishvili[89], O. Neogi, H. Ogul[90], Y. Onel, A. Penzo, C. Snyder, E. Tiras[91]

Johns Hopkins University, Baltimore, Maryland, U.S.A.

B. Blumenfeld, J. Davis, A.V. Gritsan, L. Kang, S. Kyriacou, P. Maksimovic, M. Roguljic, S. Sekhar, M.V. Srivastav, M. Swartz

The University of Kansas, Lawrence, Kansas, U.S.A.

A. Abreu, L.F. Alcerro Alcerro, J. Anguiano, S. Arteaga Escatel, P. Baringer, A. Bean, Z. Flowers, D. Grove, J. King, G. Krintiras, M. Lazarovits, C. Le Mahieu, J. Marquez, M. Murray, M. Nickel, S. Popescu[92], C. Rogan, C. Royon, S. Rudrabhatla, S. Sanders, C. Smith, G. Wilson

Kansas State University, Manhattan, Kansas, U.S.A.

B. Allmond, N. Islam, A. Ivanov, K. Kaadze, Y. Maravin, J. Natoli, G.G. Reddy, D. Roy, G. Sorrentino

JHEP12(2025)178

University of Maryland, College Park, Maryland, U.S.A.

A. Baden, A. Belloni, J. Bistany-riebman, S.C. Eno, N.J. Hadley, S. Jabeen, R.G. Kellogg, T. Koeth, B. Kronheim, S. Lascio, P. Major, A.C. Mignerey, C. Palmer, C. Papageorgakis, M.M. Paranjpe, E. Popova[93], A. Shevelev, L. Zhang

Massachusetts Institute of Technology, Cambridge, Massachusetts, U.S.A.

C. Baldenegro Barrera, J. Bendavid, H. Bossi, S. Bright-Thonney, I.A. Cali, Y.c. Chen, P.c. Chou, M. D'Alfonso, J. Eysermans, C. Freer, G. Gomez-Ceballos, M. Goncharov, G. Grosso, P. Harris, D. Hoang, G.M. Innocenti, D. Kovalskyi, J. Krupa, L. Lavezzo, Y.-J. Lee, K. Long, C. Mcginn, A. Novak, M.I. Park, C. Paus, C. Reissel, C. Roland, G. Roland, S. Rothman, T.a. Sheng, G.S.F. Stephans, D. Walter, Z. Wang, B. Wyslouch, T. J. Yang

University of Minnesota, Minneapolis, Minnesota, U.S.A.

B. Crossman, W.J. Jackson, C. Kapsiak, M. Krohn, D. Mahon, J. Mans, B. Marzocchi, R. Rusack, O. Sancar, R. Saradhy, N. Strobbe

University of Nebraska-Lincoln, Lincoln, Nebraska, U.S.A.

K. Bloom, D.R. Claes, G. Haza, J. Hossain, C. Joo, I. Kravchenko, A. Rohilla, J.E. Siado, W. Tabb, A. Vagnerini, A. Wightman, F. Yan

State University of New York at Buffalo, Buffalo, New York, U.S.A.

H. Bandyopadhyay, L. Hay, H.w. Hsia, I. Iashvili, A. Kalogeropoulos, A. Kharchilava, A. Mandal, M. Morris, D. Nguyen, S. Rappoccio, H. Rejeb Sfar, A. Williams, P. Young, D. Yu

Northeastern University, Boston, Massachusetts, U.S.A.

G. Alverson, E. Barberis, J. Bonilla, B. Bylsma, M. Campana, J. Dervan, Y. Haddad, Y. Han, I. Israr, A. Krishna, M. Lu, N. Manganelli, R. Mccarthy, D.M. Morse, T. Orimoto, A. Parker, L. Skinnari, C.S. Thoreson, E. Tsai, D. Wood

Northwestern University, Evanston, Illinois, U.S.A.

S. Dittmer, K.A. Hahn, Y. Liu, M. Mcginnis, Y. Miao, D.G. Monk, M.H. Schmitt, A. Taliercio, M. Velasco, J. Wang

University of Notre Dame, Notre Dame, Indiana, U.S.A.

G. Agarwal, R. Band, R. Bucci, S. Castells, A. Das, A. Ehnis, R. Goldouzian, M. Hildreth, K. Hurtado Anampa, T. Ivanov, C. Jessop, A. Karneyeu, K. Lannon, J. Lawrence, N. Loukas, L. Lutton, J. Mariano, N. Marinelli, I. Mcalister, T. McCauley, C. Mcgrady, C. Moore, Y. Musienko[23], H. Nelson, M. Osherson, A. Piccinelli, R. Ruchti, A. Townsend, Y. Wan, M. Wayne, H. Yockey

The Ohio State University, Columbus, Ohio, U.S.A.

A. Basnet, M. Carrigan, R. De Los Santos, L.S. Durkin, C. Hill, M. Joyce, M. Nunez Ornelas, D.A. Wenzl, B.L. Winer, B. R. Yates

JHEP12(2025)178

Princeton University, Princeton, New Jersey, U.S.A.
H. Bouchamaoui, K. Coldham, P. Das, G. Dezoort, P. Elmer, A. Frankenthal, M. Galli, B. Greenberg, N. Haubrich, K. Kennedy, G. Kopp, Y. Lai, D. Lange, A. Loeliger, D. Marlow, I. Ojalvo, J. Olsen, F. Simpson, D. Stickland, C. Tully

University of Puerto Rico, Mayaguez, Puerto Rico, U.S.A.
S. Malik, R. Sharma

Purdue University, West Lafayette, Indiana, U.S.A.
S. Chandra, R. Chawla, A. Gu, L. Gutay, M. Jones, A.W. Jung, D. Kondratyev, M. Liu, G. Negro, N. Neumeister, G. Paspalaki, S. Piperov, N.R. Saha, J.F. Schulte, F. Wang, A. Wildridge, W. Xie, Y. Yao, Y. Zhong

Purdue University Northwest, Hammond, Indiana, U.S.A.
N. Parashar, A. Pathak, E. Shumka

Rice University, Houston, Texas, U.S.A.
D. Acosta, A. Agrawal, C. Arbour, T. Carnahan, K.M. Ecklund, P.J. Fernández Manteca, S. Freed, P. Gardner, F.J.M. Geurts, T. Huang, I. Krommydas, N. Lewis, W. Li, J. Lin, O. Miguel Colin, B.P. Padley, R. Redjimi, J. Rotter, E. Yigitbasi, Y. Zhang

University of Rochester, Rochester, New York, U.S.A.
O. Bessidskaia Bylund, A. Bodek, P. de Barbaro[†], R. Demina, A. Garcia-Bellido, H.S. Hare, O. Hindrichs, N. Parmar, P. Parygin[93], H. Seo, R. Taus

Rutgers, The State University of New Jersey, Piscataway, New Jersey, U.S.A.
B. Chiarito, J.P. Chou, S.V. Clark, S. Donnelly, D. Gadkari, Y. Gershtein, E. Halkiadakis, M. Heindl, C. Houghton, D. Jaroslawski, A. Kobert, S. Konstantinou, I. Laflotte, A. Lath, J. Martins, B. Rand, J. Reichert, P. Saha, S. Salur, S. Schnetzer, S. Somalwar, R. Stone, S.A. Thayil, S. Thomas, J. Vora

University of Tennessee, Knoxville, Tennessee, U.S.A.
D. Ally, A.G. Delannoy, S. Fiorendi, J. Harris, S. Higginbotham, T. Holmes, A.R. Kanuganti, N. Karunarathna, J. Lawless, L. Lee, E. Nibigira, B. Skipworth, S. Spanier

Texas A&M University, College Station, Texas, U.S.A.
D. Aebi, M. Ahmad, T. Akhter, K. Androsov, A. Bolshov, O. Bouhali[94], A. Cagnotta, V. D'Amante, R. Eusebi, P. Flanagan, J. Gilmore, Y. Guo, T. Kamon, S. Luo, R. Mueller, A. Safonov

Texas Tech University, Lubbock, Texas, U.S.A.
N. Akchurin, J. Damgov, Y. Feng, N. Gogate, Y. Kazhykarim, K. Lamichhane, S.W. Lee, C. Madrid, A. Mankel, T. Peltola, I. Volobouev

JHEP12(2025)178

Vanderbilt University, Nashville, Tennessee, U.S.A.

E. Appelt, Y. Chen, S. Greene, A. Gurrola, W. Johns, R. Kunnawalkam Elayavalli, A. Melo, D. Rathjens, F. Romeo, P. Sheldon, S. Tuo, J. Velkovska, J. Viinikainen, J. Zhang

University of Virginia, Charlottesville, Virginia, U.S.A.

B. Cardwell, H. Chung, B. Cox, J. Hakala, R. Hirosky, M. Jose, A. Ledovskoy, C. Mantilla, C. Neu, C. Ramón Álvarez

Wayne State University, Detroit, Michigan, U.S.A.

S. Bhattacharya, P.E. Karchin

University of Wisconsin — Madison, Madison, Wisconsin, U.S.A.

A. Aravind, S. Banerjee, K. Black, T. Bose, E. Chavez, S. Dasu, P. Everaerts, C. Galloni, H. He, M. Herndon, A. Herve, C.K. Koraka, S. Lomte, R. Loveless, A. Mallampalli, A. Mohammadi, S. Mondal, T. Nelson, G. Parida, L. Pétré, D. Pinna, A. Savin, V. Shang, V. Sharma, W.H. Smith, D. Teague, H.F. Tsoi, W. Vetens, A. Warden

Authors affiliated with an international laboratory covered by a cooperation agreement with CERN

S. Afanasiev, V. Alexakhin, Yu. Andreev, T. Aushev, D. Budkouski, R. Chistov[95], M. Danilov[95], T. Dimova[95], A. Ershov[95], S. Gninenko, I. Gorbunov, A. Gribushin[95], A. Kamenev, V. Karjavine, M. Kirsanov, V. Klyukhin[95], O. Kodolova[96], V. Korenkov, A. Kozyrev[95], N. Krasnikov, A. Lanev, A. Malakhov, V. Matveev[95], A. Nikitenko[97,96], V. Palichik, V. Perelygin, S. Petrushanko[95], S. Polikarpov[95], O. Radchenko[95], M. Savina, V. Shalaev, S. Shmatov, S. Shulha, Y. Skovpen[95], V. Smirnov, O. Teryaev, I. Tlisova[95], A. Toropin, N. Voytishin, B.S. Yuldashev[†,98], A. Zarubin, I. Zhizhin

Authors affiliated with an institute formerly covered by a cooperation agreement with CERN

E. Boos, V. Bunichev, M. Dubinin[86], V. Savrin, A. Snigirev, L. Dudko, K. Ivanov, V. Kim[23], V. Murzin, V. Oreshkin, D. Sosnov

[†] *Deceased*
[1] *Also at Yerevan State University, Yerevan, Armenia*
[2] *Also at TU Wien, Vienna, Austria*
[3] *Also at Ghent University, Ghent, Belgium*
[4] *Also at Universidade do Estado do Rio de Janeiro, Rio de Janeiro, Brazil*
[5] *Also at FACAMP — Faculdades de Campinas, Sao Paulo, Brazil*
[6] *Also at Universidade Estadual de Campinas, Campinas, Brazil*
[7] *Also at Federal University of Rio Grande do Sul, Porto Alegre, Brazil*
[8] *Also at The University of the State of Amazonas, Manaus, Brazil*
[9] *Also at University of Chinese Academy of Sciences, Beijing, China*
[10] *Also at China Center of Advanced Science and Technology, Beijing, China*
[11] *Also at University of Chinese Academy of Sciences, Beijing, China*
[12] *Also at School of Physics, Zhengzhou University, Zhengzhou, China*
[13] *Now at Henan Normal University, Xinxiang, China*

JHEP12(2025)178

[14] *Also at University of Shanghai for Science and Technology, Shanghai, China*
[15] *Now at The University of Iowa, Iowa City, Iowa, U.S.A.*
[16] *Also at Center for High Energy Physics, Peking University, Beijing, China*
[17] *Also at Cairo University, Cairo, Egypt*
[18] *Also at Suez University, Suez, Egypt*
[19] *Now at British University in Egypt, Cairo, Egypt*
[20] *Also at Purdue University, West Lafayette, Indiana, U.S.A.*
[21] *Also at Université de Haute Alsace, Mulhouse, France*
[22] *Also at Istinye University, Istanbul, Turkey*
[23] *Also at an institute formerly covered by a cooperation agreement with CERN*
[24] *Also at University of Hamburg, Hamburg, Germany*
[25] *Also at RWTH Aachen University, III. Physikalisches Institut A, Aachen, Germany*
[26] *Also at Bergische University Wuppertal (BUW), Wuppertal, Germany*
[27] *Also at Brandenburg University of Technology, Cottbus, Germany*
[28] *Also at Forschungszentrum Jülich, Juelich, Germany*
[29] *Also at CERN, European Organization for Nuclear Research, Geneva, Switzerland*
[30] *Also at HUN-REN ATOMKI — Institute of Nuclear Research, Debrecen, Hungary*
[31] *Now at Universitatea Babes-Bolyai — Facultatea de Fizica, Cluj-Napoca, Romania*
[32] *Also at MTA-ELTE Lendület CMS Particle and Nuclear Physics Group, Eötvös Loránd University, Budapest, Hungary*
[33] *Also at HUN-REN Wigner Research Centre for Physics, Budapest, Hungary*
[34] *Also at Physics Department, Faculty of Science, Assiut University, Assiut, Egypt*
[35] *Also at The University of Kansas, Lawrence, Kansas, U.S.A.*
[36] *Also at Punjab Agricultural University, Ludhiana, India*
[37] *Also at University of Hyderabad, Hyderabad, India*
[38] *Also at Indian Institute of Science (IISc), Bangalore, India*
[39] *Also at University of Visva-Bharati, Santiniketan, India*
[40] *Also at IIT Bhubaneswar, Bhubaneswar, India*
[41] *Also at Institute of Physics, Bhubaneswar, India*
[42] *Also at Deutsches Elektronen-Synchrotron, Hamburg, Germany*
[43] *Also at Isfahan University of Technology, Isfahan, Iran*
[44] *Also at Sharif University of Technology, Tehran, Iran*
[45] *Also at Department of Physics, University of Science and Technology of Mazandaran, Behshahr, Iran*
[46] *Also at Department of Physics, Faculty of Science, Arak University, ARAK, Iran*
[47] *Also at Helwan University, Cairo, Egypt*
[48] *Also at Italian National Agency for New Technologies, Energy and Sustainable Economic Development, Bologna, Italy*
[49] *Also at Centro Siciliano di Fisica Nucleare e di Struttura Della Materia, Catania, Italy*
[50] *Also at James Madison University, Harrisonburg, Maryland, U.S.A.*
[51] *Also at Università degli Studi Guglielmo Marconi, Roma, Italy*
[52] *Also at Scuola Superiore Meridionale, Università di Napoli 'Federico II', Napoli, Italy*
[53] *Also at Fermi National Accelerator Laboratory, Batavia, Illinois, U.S.A.*
[54] *Also at Lulea University of Technology, Lulea, Sweden*
[55] *Also at Consiglio Nazionale delle Ricerche — Istituto Officina dei Materiali, Perugia, Italy*
[56] *Also at UPES — University of Petroleum and Energy Studies, Dehradun, India*
[57] *Also at Institut de Physique des 2 Infinis de Lyon (IP2I), Villeurbanne, France*
[58] *Also at Department of Applied Physics, Faculty of Science and Technology, Universiti Kebangsaan Malaysia, Bangi, Malaysia*
[59] *Also at Trincomalee Campus, Eastern University, Sri Lanka, Nilaveli, Sri Lanka*
[60] *Also at Saegis Campus, Nugegoda, Sri Lanka*
[61] *Also at National and Kapodistrian University of Athens, Athens, Greece*
[62] *Also at Ecole Polytechnique Fédérale Lausanne, Lausanne, Switzerland*
[63] *Also at Universität Zürich, Zurich, Switzerland*

JHEP12(2025)178

[64] Also at Stefan Meyer Institute for Subatomic Physics, Vienna, Austria
[65] Also at Near East University, Research Center of Experimental Health Science, Mersin, Turkey
[66] Also at Konya Technical University, Konya, Turkey
[67] Also at Izmir Bakircay University, Izmir, Turkey
[68] Also at Adiyaman University, Adiyaman, Turkey
[69] Also at Bozok Universitetesi Rektörlügü, Yozgat, Turkey
[70] Also at Istanbul Sabahattin Zaim University, Istanbul, Turkey
[71] Also at Marmara University, Istanbul, Turkey
[72] Also at Milli Savunma University, Istanbul, Turkey
[73] Also at Informatics and Information Security Research Center, Gebze/Kocaeli, Turkey
[74] Also at Kafkas University, Kars, Turkey
[75] Now at Istanbul Okan University, Istanbul, Turkey
[76] Also at Hacettepe University, Ankara, Turkey
[77] Also at Erzincan Binali Yildirim University, Erzincan, Turkey
[78] Also at Istanbul University — Cerrahpasa, Faculty of Engineering, Istanbul, Turkey
[79] Also at Yildiz Technical University, Istanbul, Turkey
[80] Also at School of Physics and Astronomy, University of Southampton, Southampton, United Kingdom
[81] Also at Monash University, Faculty of Science, Clayton, Australia
[82] Also at Bethel University, St. Paul, Minnesota, U.S.A.
[83] Also at Università di Torino, Torino, Italy
[84] Also at Karamanoğlu Mehmetbey University, Karaman, Turkey
[85] Also at California Lutheran University;, Thousand Oaks, California, U.S.A.
[86] Also at California Institute of Technology, Pasadena, California, U.S.A.
[87] Also at United States Naval Academy, Annapolis, Maryland, U.S.A.
[88] Also at Bingol University, Bingol, Turkey
[89] Also at Georgian Technical University, Tbilisi, Georgia
[90] Also at Sinop University, Sinop, Turkey
[91] Also at Erciyes University, Kayseri, Turkey
[92] Also at Horia Hulubei National Institute of Physics and Nuclear Engineering (IFIN-HH), Bucharest, Romania
[93] Now at another institute formerly covered by a cooperation agreement with CERN
[94] Also at Hamad Bin Khalifa University (HBKU), Doha, Qatar
[95] Also at another institute formerly covered by a cooperation agreement with CERN
[96] Also at Yerevan Physics Institute, Yerevan, Armenia
[97] Also at Imperial College, London, United Kingdom
[98] Also at Institute of Nuclear Physics of the Uzbekistan Academy of Sciences, Tashkent, Uzbekistan

JHEP12(2025)178